2015

Wedge failure analysis of anchored rock slopes subjected to surcharge and seismic loads

Yan Kou

Edith Cowan University

Copyright Warning

Wedge Failure Analysis of Anchored Rock Slopes Subjected to Surcharge and Seismic Loads

By

YAN KOU

Associate Professor Sanjay Kumar Shukla, Principal Supervisor

Dr. Hang Vu, Associate Supervisor

This thesis is presented in fulfillment of the requirements for the degree of

Master of Engineering Science

November 2015

School of Engineering

Faculty of Health, Engineering and Science

EDITH COWAN UNIVERSITY

Use of Thesis

Abstract

Slope stability in mining and civil engineering projects is always a problem of great concern. Because the rock mass behavior is significantly governed by the presence of joints or other discontinuities, several types of slope failure, such as plane failure, wedge failure, toppling failure, buckling failure and circular failure, are often observed. The present work focuses on the study of the wedge failure, which occurs as sliding of a mass of rock on two intersecting planes, generally discontinuity planes.

Recently, the factor of safety of rock slopes against the wedge failure has been studied in a number of investigations under static and/or dynamic conditions by different methods such as the limit equilibrium method, numerical modeling method, reliability method and stereographic method. However, the anchored rock slope against the wedge failure subjected to surcharge and seismic load has not yet been studied in detail in earlier studies.

In this thesis, the rock slope subjected to the generalized loads such as surcharge and seismic/dynamic loads is analyzed against the wedge failure by the limit equilibrium method. The expression for the factor of safety was derived for the cases with anchors and without anchors separately. In addition, a parametric study is carried out to demonstrate the effects of the most relevant governing parameters on the stability of rock slope. The parameters include geometrical parameters, joint material properties, unit weight of rock, anchor inclination and hydraulic parameters. Several special cases of the developed generalized expression result in the expressions for the factor of safety for simplified field situations as reported in the literature.

The parametric study shows that most parameters as mentioned above affect the factor of safety (FS) of the rock slope against the wedge failure significantly. In order to find an easy way to work on the parametric analysis, the "*" indicates dimensionless parameters. It is observed that the surcharge would always be a destabilizing force when the cohesion (c^*) is not zero; the FS decreases with an increase in surcharge. However, when $c^* = 0$, the FS increases slightly with an increase in surcharge. The anchor forces (T^*) would always be a stabilizing force that makes the FS increase with an increase in T^*. As the angle of

inclination of the joint plane/failure plane to the horizontal (ψ_p) increases, the FS increases nonlinearly; it increase sharply by 60% from 42° to 45° while it deceases nonlinearly by 67% with an increase in the slope angle (ψ_f) from 40° to 60°. It is also observed that the FS decreases with an increase in horizontal seismic acceleration coefficient (k_h) and the vertical seismic acceleration coefficient (k_v), separately, while it increases linearly with an increase in the following parameters: the cohesion (c^*) and the angle of shearing resistance (ϕ), separately. The FS increases with an increase in inclination of stabilizing force to the normal at the failure plane (α); it becomes maximum when α increases to 80°. However, the unit weight of rock (γ^*) does not affect the FS significantly.

Acknowledgements

First and foremost I would like to thank my supervisor Associated Professor Sanjay Kumar Shukla for his support, time and advice that I have received during the writing of my thesis. I would also like to take time to thank him to introducing me to research, and leading me into this complicated field. Without his helpful comments and suggestions this thesis may have been written very differently.

I would also like to thank my associate supervisor Dr. Hang Vu for his assistance in editing the thesis, and of course his wise words and comments. I would also like to thank any colleagues and friends for their helpful thoughts and guidance. Their past knowledge and experience has been very helpful in the writing of this thesis.

Through the writing of this thesis I have had the pleasure in meeting many new people and without these people this thesis could not have been written. I am forever in gratitude to them.

Yan Kou

The declaration page
is not included in this version of the thesis

Notation

A	total area of joint plane (m^2)
A_1	area of joint plane 1 (m^2)
A_2	area of joint plane 1 (m^2)
A_c	the cross-section area of wedge block (m^2)
B	length of PY , which in the Fig.1 (b)
c	cohesion along sliding surface (N/m^2)
c^*	cohesion alone sliding surface ($c / \gamma H$) (dimensionless)
D	length of PR , which in the Fig.1 (b)
F_r	resisting force (N)
F_i	driving force (N)
FS	factor of Safety against sliding (dimensionless)
H	height of the slope (m)
k_v	vertical seismic acceleration coefficient (dimensionless)
k_h	horizontal seismic acceleration coefficient (dimensionless)
L_1	a side of plane 1 (OR) (m)
L_2	a side of plane 2 (OP) (m)
L_{12}	intersection line of wedge block (OE) (m)
N	normal force acting on the intersection line (N)
N_1	normal force acting on the joint plan 1 (N)
N_2	normal force acting on the joint plan 2 (N)
Q	load on the wedge block due to surcharge (N)
q	surcharge (N/m^2)

q^*	surcharge ($= q/\gamma h$) (dimensionless)
S	force of shearing resistance (N)
T	dimensionless the forces of anchors (N)
T^*	the forces of anchors ($= T/\gamma h^3$)
U	total water pressure along joint plane (N)
U_1	water pressure along joint plane (N)
U_2	water pressure along joint plane (N)
W	weight of the sliding block (N)
α	the inclination of stabilizing force to the normal at the failure plane (degrees)
ψ_p	angle of inclination of the joint plane/failure plane to the horizontal (degrees)
ψ_f	angle of inclination of the slope face to the horizontal (degrees)
ϕ	friction angle (degrees)
γ	unit weight of the rock (N/m^3)
γ_w	unit weight of water (N/m^3)
γ^*	unit weight of rock ($= \gamma/\gamma_w$)(dimensionless)
λ	wedge factor by Kovari and Fritz (1975) (dimensionless)
θ_1	angle between L_1 and L_{12} (m)
θ_2	angle between L_2 and L_{12} (m)
ω_1	the angle between the surface A and vertical (degree)
ω_2	the angle between the surface B and vertical (degree)

List of Figures

Contents

Chapter 1

Introduction

1.1 General

Slope stability analysis is a study of much importance for many industry areas, such as buildings, bridges, dams, highways, railways and mines. They should be designed as safe as possible by engineers, due to the impact on personnel safety and great cost of any potential accidents. The slope failure may trigger a disaster as well. That is why this subject has been studied by many engineers and researchers for centuries. The angle of inclination of the slope face to the horizontal affects the economy and safety. A small angle of slope means extra excavation and extra mine waste, but too steep a slope will cause a safety problem, and will increase the probability of failure. Therefore the balance between those two factors will have to be considered when thinking about economic factors and safety concerns. Most current systems for designing slopes in open pit mines assume that the principle of limiting equilibrium and kinematical applications are followed and that the rock can be treated as a typical engineering material. However, the rock is not a typical engineering material on a macroscopic level hence a factor of safety approach is adopted (Hoek and Bray, 1981; Stacey, 1996).

Rock slope failure is generally governed by the intercalated change in lithologies and the correlative change in discontinuities such as bedding, faults, foliation cleavage schistosity and joints. (Wyllie and Mah, 2004). While the rotational rock failure can occur under highly weathering and rock mass, the rock slope failures have been identified by engineers in 5 types of categories: 1) plane failure, 2) circular failure, 3) wedge failure, 4) toppling failure and 5) buckling failure.

The rock mass sliding on a single surface of rock slope is termed as the plane failure, it generally occurs in hard or soft rocks with well-defined discontinuities and joints, e.g., layered sedimentary rock, volcanic flow rocks, block-jointed granite, foliated metamorphic

rock. The sliding rotation of a rock mass about an edge, either single or multiple blocks is termed as toppling failure. Toppling failure is possible whenever a set of well-developed or through-going discontinuities dips steeply into the slope. Buckling failure takes place when the excavation is carried out with its face parallel to the thin weakly bonded and steeply dipping layers, which may buckle and fracture near the toe, resulting in the sliding of the upper portions of the layers. (Goodman and Kieffer， 2000)

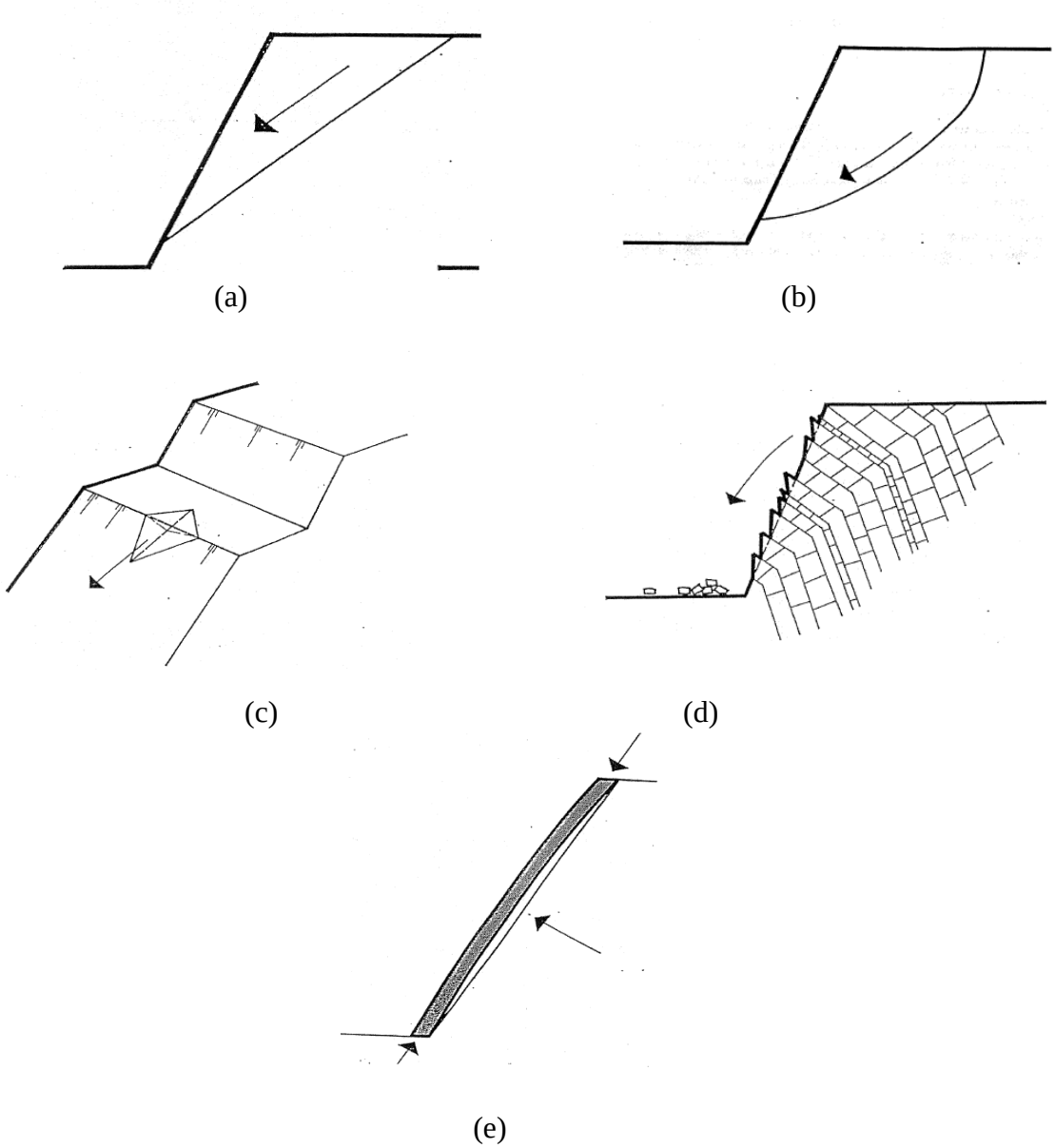

Fig. 1.1. Types of rock slope failure: (a) plane failure, (b) circular failure, (c) wedge failure, (d) toppling failure, and (e) buckling failure. (adapted from Hoek and Bray, 1981; Goodman, 1989; Kliche, 1999; Wyllie and Mah, 2004)

The wedge failure of rock slope is probably the most common type of failure in rock sliding (Hoek and Bray, 1981). The tetrahedron wedge failure can occur in one of following way (Piteau and Martin，1982):

- by sliding on both planes in a direction along the line of intersection
- by sliding along one plane only with separation across the other plane
- by rotational sliding on one plane and separation across the other plane
- by progressive raveling of rock along planes formed by the wedge in highly jointed rock

In most studies presented so far, the main efforts have been made so to consider several different methods to analyse the wedge failure. The stereographic method is first presented by Hoek *et al.* (1973) and it is a close – form method by (Low and Einstein, 1992). The limiting equilibrium method is the most popular approach applied in investigation. Despite of the surcharge load involved in stability of rock slope against plane failure that was presented by Shukla *et al.* (2009), the wedge failure of rock slope has not received proper attention until recently. It is the purpose of this thesis to analyses the effect of surcharge load on the rock slope against wedge failure by developing an expression for the factor of safety through the anchoring system. The parametric study will be carried out by incorporating most of the practically occurring destabilizing forces as well as an external stabilizing force.

1.2 Objectives and scope of the research

The analysis based on the limiting equilibrium method has been widely used by the engineers and the researchers for a long period. As the previous research works successfully, this method has been well accepted, because the accuracy of this method has been compared with numerical method and other method, such as kinematic method, vector algebra method and closed-form equations method. As some researchers have not presented the expression of the factor of safety of rock slope against the wedge failure involving some field aspects, such as surcharge and anchor force. These areas are considered for further research in order to

analysis the effects of the factor of safety.

This research aims at investigating the wedge failure of rock slope under seismic load and water force. In order to cope with the research problem, which is identified above, the research aims to achieve the following outcomes:

- deriving new expression of factor of safety under the seismic load and the water force against the wedge failure without anchors
- illustrating the analysis of anchored rock slope against the wedge failure
- developing the expression for anchored rock slope against the wedge failure
- analyzing the anchored rock slope subjected surcharge and seismic load against the wedge failure
- using the graphical method to analyse the special cases in view of different practical situations
- analyzing the effect of parameters governing the rock slope stabilize

The factor of safety is the ratio of the sum of the resisting forces to the sum of the driving forces which act on the considered slope. Ideally, the factor of safety greater than unity means that the slope would not slide; otherwise the slope has the potential of failing in the future. FHWA (1989) reported that a factor of safety of 1.3 is adequate for low slopes and a factor of safety of 1.5 is required for critical slopes adjacent to major highways. The factor of safety can not only express the failure probability, but also it is easy to calculate for real projects, where the stabilizing of rock slopes has always been a challenging problem for mining and civil engineering.

Seismic loading means application of an earthquake-generated agitation to a structure. They are represented as horizontal and vertical forces, equal to weight of the potential sliding mass multiplied by a coefficient. They happen at contact surfaces of a structure either with the ground, or with adjacent structures, or with gravity waves from tsunami.

Sometimes, the seismic load exceeds the ability of a structure to resist it without being broken, partially or completely due to their mutual interaction, seismic loading and seismic performance of a structure are intimately related.

1.3 Organization of the present work

In this chapter, the research area is introduced and basic information of the concerned subject is described. A critical review of the previous studies on static stability, dynamic stability, numerical modeling, reliability and stereographic analyses are presented in Chapter 2, and subsequently the research problem is identified. Chapter 3 describes the analytical formulation of the identified problem to determine the analytical expression for the factor of safety of rock slope without anchors along with a discussion of its special cases in view of different practical situations. In Chapter 4, the parametric studies for the stability of rock slope without anchors are presented, the analysis focuses on the effects of surcharge on the factor of safety with different value for the parameters. Chapter 5 describes the derivation of the analytical expression for factor of safety of rock slope with anchors and presents some discussion. In Chapter 6, the parametric studies for the stability of rock slope with anchors are presented. Moreover, in Chapter 6 the parametric study not only analyses the effect of stabilizing force for the factor of safety, but also analyses the most governing parameters that affects for the factor of safety. The summary of the conducted work in the thesis and the conclusions and further research problems are presented in Chapter 7.

Chapter 2

Literature Review

2.1 General

In rock slope stability analysis area, the researchers have made efforts for several decades. A rock mass generally exhibits anisotropic and heterogeneous behaviors. The behaviors are governed by the joints and other discontinuities. The engineers classify the failure of rock slope in five different types: plane failure, wedge failure, buckling failure, toppling failure and circular failure. There are several methods that can be used to analyse the stability of rock slopes, such as limit equilibrium method, stereographic method, numerical method and vector method, etc. This chapter attempts to categorize the literature in five sections, namely: static stability analysis, dynamic stability analysis, numerical modeling analysis, reliability analysis and stereographic analysis.

2.2 Static stability analysis

The analysis of static slope stability is based on the static equilibrium of unstable rock mass. In static system, the sum of each direction of forces and moments is equal to zero. The limit equilibrium method is presented by Hoek and Bray (1973) for the analysis of wedge failures.

The factor of safety (FS) is defined as the ratio of resisting force to the driving force. Thus:

$$FS = \frac{\text{Resisting force}}{\text{Driving force}} \tag{2.1}$$

Assuming that sliding is resisted only by the friction and that the friction angle ϕ is same for both planes, the following equation holds:

$$FS = \frac{(R_A + R_B)\tan\phi}{W\sin\phi} \tag{2.2}$$

where R_A and R_B are the normal reaction forces provided by plane A and plane B, respectively, as given below:

$$R_A \sin\left(\beta - \frac{1}{2}\xi\right) = R_B \sin\left(\beta + \frac{1}{2}\xi\right) \tag{2.3}$$

$$R_A \sin\left(\beta - \frac{1}{2}\xi\right) + R_B \sin\left(\beta + \frac{1}{2}\xi\right) = W\cos\psi_i \tag{2.4}$$

$$R_A + R_B = \frac{W\cos\psi_i \sin\beta}{\sin\frac{\xi}{2}} \tag{2.5}$$

where the angles β and ξ are defined in Figure 2.1(a). Angles β and ξ are measured on the great circle containing the pole to the line of intersection and the poles of the two slide planes.

Hence,

$$FS = \frac{\sin\beta}{\sin\frac{\xi}{2}} \frac{\tan\phi}{\tan\psi_i} \tag{2.6}$$

In other words,

$$FS_W = KFS_P \tag{2.7}$$

where FS_W is the factor of safety against the wedge failure, FS_P is the factor of safety against the plane failure, ψ_i is the dip angle as the line of intersection, and K is the wedge factor.

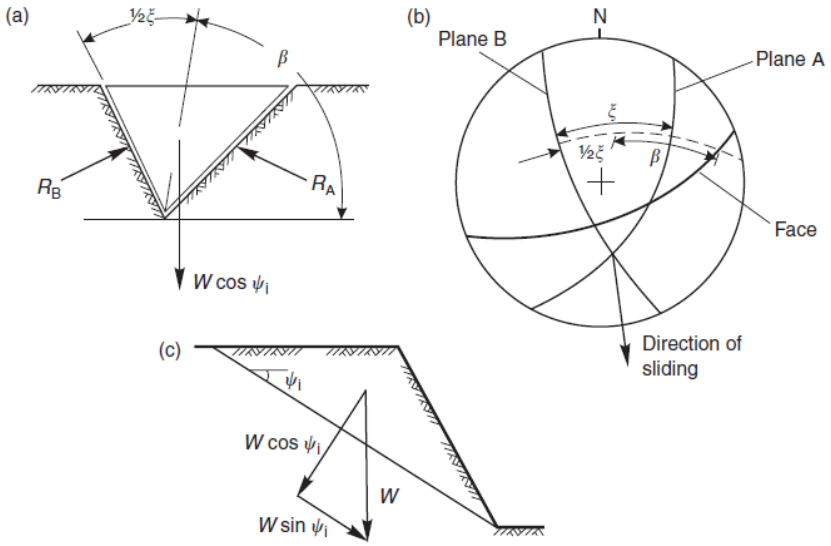

Fig. 2.1. Resolution of forces to calculate factor of safety of wedge: (a) view of wedge looking at face showing definition of angles β and ξ, and reactions on sliding planes R_A and R_B; (b) stereonet showing measurement of angles β and ξ; (c) cross-section of wedge showing resolution of wedge weight W (after Wyllie and Mah, 2005)

Wang *et al.* (2004) proposed a general limit equilibrium method based on the Pan's "Maximum principle" and the upper bound method to determine the direction of shear force. A non-symmetric wedge and a symmetric wedge were analyzed using two methods on the basis of which the formulation has been derived. After that, the influence is considered on stability due to the direction of the shear force acting on the two discontinuities and it also be identified by the finite – element analysis. Finally, the two comparisons have been applied; one comparison takes place within the traditional limit equilibrium or the method of general limit, upper bound and dilatancy of discontinuous plane, the other is the comparison of the finite element method with the method of traditional limit equilibrium and the general limit

equilibrium method.

Alejano *et al.* (2011) proposed three footwall failures of rock slope such as bilinear slab failure, ploughing slab failure and three hinge buckling failure. They are not commonly encountered failures as we have known, such as plane failure, wedge failure, toppling failure and circular failure. The paper shows the analysis of bilinear slab failure and ploughing slab failure in 2 different conditions according to whether discontinuity control is full or partial. The limit equilibrium method has been carried out for factor of safety for two failure types in different phenomenon, and the methodologies of numerical modeling approach and physical modeling approach have been explained by the authors in order to compare the theoretical results of these two failures to justify the feasibility of limit equilibrium method.

Bobet (1999) stated the analytical solution of toppling failure on the basis of the limiting equilibrium approach. In this investigation, the toppling mechanism was analyzed in 2D – plane conditions, and also consideration is the stability of toppling failure with water seepage. A numerical method which was proposed by Hoek and Bray (1981) has been implemented for compare analytical results, as the result of comparison the accuracy has been given as under 10% of the numerical solution, for height and length ratios larger than 50.

Adhikary *et al.* (1997) investigated the mechanism of flexural toppling failure of rock slopes by implemented centrifuge test and compared it with the theoretical model based on a limiting equilibrium approach (Aydan and Kawamoto, 1992). In the centrifuge experiments, seven tests were performed using three different techniques which are quartz sand mixed with 2% Portland cement, fibre-cement and a mixture of limonite and 15% gypsum on top of each layers. The crack was found to be oriented at an angle varying from 12° to 20° above the normal to the joint dip angle. Based on the analytical model, a set of designs charts have been set up to help with analysis of flexural toppling slope. After comparing, the accurate result was found corresponding to the expected result of failure load for the each tests presented in this study. That was mean the limiting equilibrium method which take into account of toppling failure will a capable approach to predict future fracture surface.

2.3 Rock sliding induced by dynamic force

Due to the earthquakes and blasting shaking, rock slope dynamic forces can be categorized as horizontal or vertical seismic forces. The force would be equal to the weight of the potential sliding mass multiplied by a coefficient. This is a common approach that is carried by engineers to analyse the seismic response of rock slope.

Ling and Cheng (1997) analysed the rock sliding induced by the seismic force. They presented a formula that is based on the two – dimensional limit equilibrium analysis. It is valid for a rock mass with sufficiently large width, typically with a plane strain condition. The rock mass is considered as a rigid body. The strength of the joint plane is assumed to be plastic, obeying the coulomb failure criterion. As the figure shows below, it is noted that the horizontal and vertical seismic forces are considered to be positive when acting horizontally away from the slope and vertically in the direction of gravity. The expression for the factor of safety is given below:

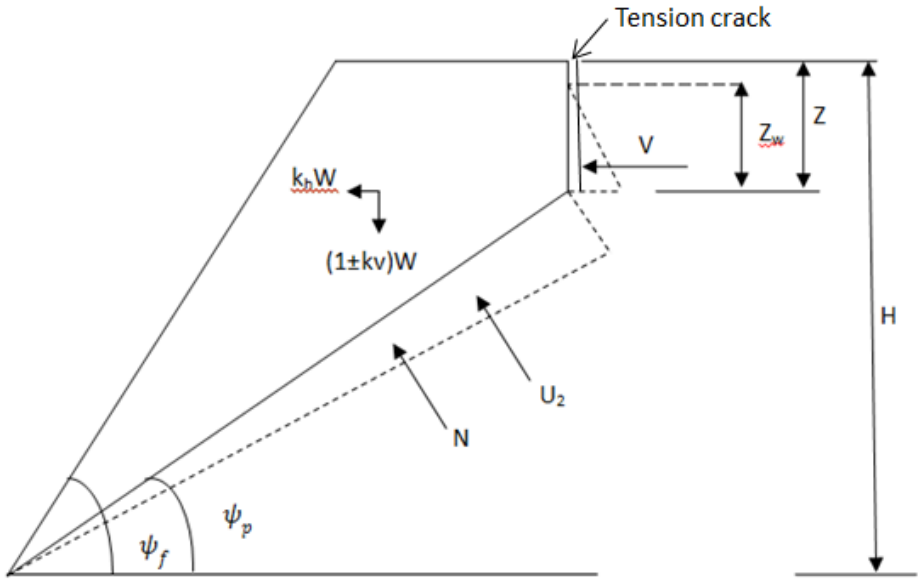

Fig. 2.2. Mechanism of rock slope against plan failure with tension crack under self-weight, water forces, and horizontal and vertical seismic forces

$$FS = \frac{W\cos(\psi_p + \theta)\tan\phi - \left[V(\sin\psi_p + U)\tan\phi - C\right]/k}{W\sin(\psi_p + \phi) + (V\cos\psi_p)/k} \tag{2.8}$$

$$\tan\theta = \frac{k_h}{1 + k_v} \tag{2.9}$$

where

ψ_P = angle of inclination of the joint plane/failure plane to the horizontal

ψ_f = angle of inclination of the joint plane/failure plane to the horizontal

V = horizontal force due to the water pressure in the tension crack

U = uplift force due to the water pressure on failure plane

ϕ = joint plane friction angle

θ = function of seismic coefficients

c = total cohesive force acting along joint plane

Shukla and Hossain (2011) presented an expression for the factor of safety of multi-directional anchored rock slope subjected to the surcharge and seismic loads. The parametric study approach which was used to analyze special cases, such as the inclination of slope face, the inclination of the failure plane, the depth of the tension crack, the depth of water in tension crack, the shear strength parameters of the material at the failure plane, the unit weight of rock, the stabilizing force and its inclination, and the seismic force. This study is also shown as a graphical analysis of any specific inclination of one set of anchors to the normal at failure plane, when the second set of anchors are greater than about 60 degree where the factor of safety does not change significantly.

Basha *et al.* (2013) proposed the stability analysis of rock slopes against the wedge failure subject to the seismic loads on basis of Barton's theory. They developed an approach or a methodology of expression of factor of safety of the sliding block. The formulation is showed below as:

$$F_R = R_{na} \tan\left[\left(JRC \log\left(\frac{JCS}{\sigma_{na}}\right) + \phi_r \right)\right] + R_{nb} \tan\left[\left(JRC \log\left(\frac{JCS}{\sigma_{nb}}\right) + \phi_r \right)\right] \quad (2.10)$$

$$F_D = W \sin\delta_s + k_h \cos\delta_s - k_v \sin\delta_s + U_1 \cos\delta_s \quad (2.11)$$

$$FOS = \frac{F_R}{F_D} \quad (2.12)$$

where

F_R = resisting force

F_D = driving force

R_{na}, R_{nb} = net reaction force on plane A and B, respectively

JRC = joint roughness coefficient

JCS = joint compressive strength

k_v, k_h = vertical and horizontal seismic acceleration coefficient, respectively

ϕ_r = residual friction angle

σ_{na}, σ_{nb} = stress on plane A and B, respectively

The load and resistance factors have been estimated by the target reliability approach. The consideration of parameter input and variation of coefficient has been applied to prove that the load resistance factor design is a capable approach of handling multiple design parameters. They concluded conclusion from this study that the resistance factor decrease when the coefficient of variation of JRC and JCS increase, while the load factor rise particularly in corresponding to the horizontal seismic acceleration coefficient.

Kumsar *et al.* (2000) provided an experiment to show the model wedges under static and dynamic loading conditions and the existing limiting equilibrium methods were derived to take into account the dynamic effects. The expression of the factor of safety is obtained as:

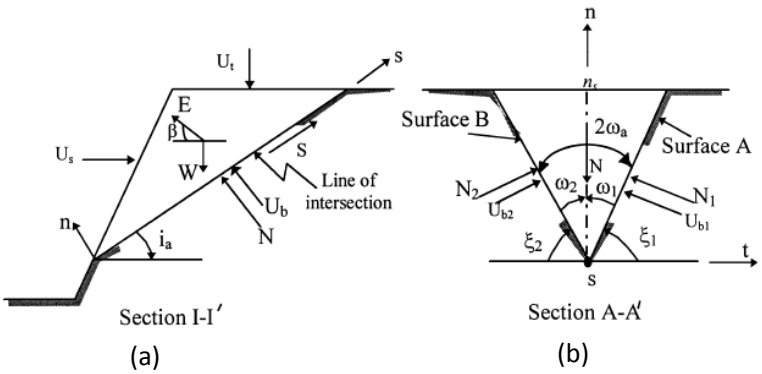

Fig. 2.3. Force acting on a wedge block (after Kumsar, 2000). (a) side view of slope, (b) front view of slope

$$FS = \frac{\left[\lambda\left[W\left(\cos i_a - \eta\sin\left(i_a+\beta\right)\right)+U_s\sin i_a + U_t\cos i_a\right]-\alpha U_b\right]\tan\phi + c\left(A_1+A_2\right)}{W\left(\sin i_a + \eta\cos\left(i_a+\beta\right)\right)-U_s\cos i_a + U_t\sin i_a} \qquad (2.13)$$

where

U_s, U_t = the water force acting on the face and the upper fart of the slope, respectively.

i_a, β = the plunge of the intersection line and the inclinations of the dynamic force E

α = Biot's coefficient

λ = called the wedge factor by Kovari and Fritz (1975)

c, ϕ = cohesion and friction angle, respectively

A_1, A_2 = area of plane A and plane B, respectively

W, η = weight of the wedge block W, and the seismic coefficient

The above presented method was checked through the laboratory tests being performed under the well-controlled conditions and by the actual cases being studied. Six types of concrete wedge block and base were prepared by the authors to test them under 4 different conditions such as static test, dry test, submerged test and dynamic test. A shaking table was used for the dynamic test under dry condition and static test were carried out under dry and submerged conditions. After that comparison of the experimental and theoretical result proved that the limiting equilibrium method is valid. Finally, 5 cases had been studied to

check the validity of the present method in the paper.

Aydan and Kumsar (2010) developed the expression evaluating the displacement of sliding of rock wedges subject to the dynamic and water loading. They derived the solution through numerical integration method. The solution was also based on the linear acceleration finite difference technique. The function of velocity, displacement and acceleration of wedge for a time step also had been presented by the authors. They compared the results with that of experimental approach being same as shown in previous paper (Kumsar *et al.* 2000), as the figure shows that good accuracy was observed between the experimental results and the analytical evaluation.

2.4 Numerical modeling method of analysis slope stability

He *et al.* (2013) presented a three-dimensional numerical modeling method for rock slope stability, which codes numerical manifold method (NMM). This method is like the combination of the finite element method with the discontinuous deformation analysis, thus providing another version of hybrid modeling. They explained the fundamental concepts, framework and algorithm of NMM, so as to compare the 3-D NMM with the analytical result to identify if the 3-D NMM is an accurate method for jointed rock slope stability analysis. This investigation has found that 3-D NMM is a convenient geometrical modeling and has a good capability to use in stability analysis.

Goodman and Kieffer (2000) stated the principles of rock failure, and explained how and why different failure modes occurred in different rocks. The paper explained that the surface excavation is more dangerous than that underground, because of weathered, water active and tangential stress at first. Recognition of rock slope hazards had been illustrated and explained in 8 different situations with figures; the authors also plotted a table for different failure mode and discussed how different failures worked and developed in rock slope. Stability analysis had been roughly presented; 3D and 2D had been considered under limit equilibrium approach corresponded with numerical models, such as UDEC, DDA, AND FLAC. A real case had been shown in this paper, which is rock slope failure along spillway of Pardee dam in California that illustrated the diversity of behavioral styles to which a rock slope is susceptible.

2.5 Reliability study of rock slope

Tamimi *et al.* (1988) proposed the reliability study of rock slope against single plane sliding subjected the water force. They found the problem of the previous method of reliability analysis of rock slope to derived a new approach which including possible correlations that between the basic random variables involved in the design equation. Two popular approaches had been described briefly at first which are Central Limit Theorem and Convolution Integral. The other simulation technique had been explained more detailed which is Monte Carlo simulation, and also pointed out the deficiency of no consideration of correlations between the basic random variables. Therefore, that was modified in this paper to determine the reliability of rock slope. The expression and influence diagram were presented by authors as:

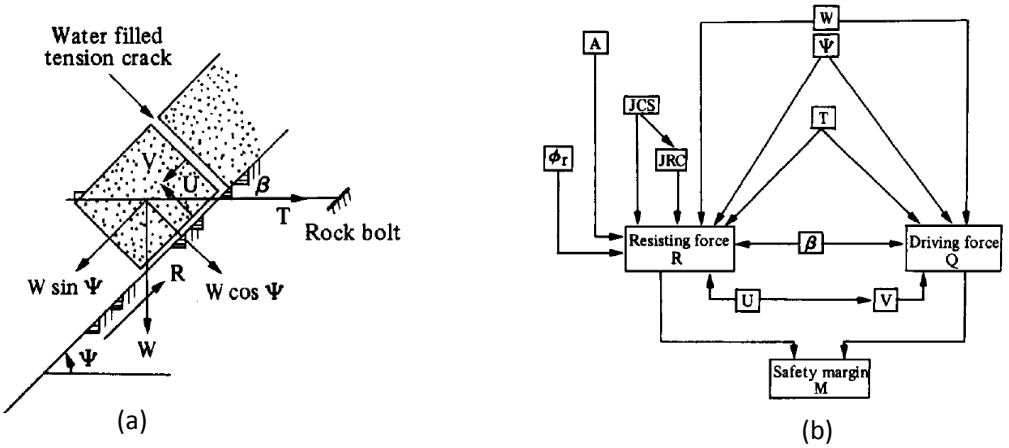

Fig. 2.4. Plane sliding and proposed influence diagram (after Tamimi *et al.*, 1988)

$$FS = \frac{R}{Q} = \frac{\left[T\sin\beta + W\cos\psi - U\right]\tan\left[JRC\log_{10}\left(\frac{JCS \bullet A}{W\cos\psi + T\sin\beta - U}\right) + \phi_r\right]}{W\sin\psi - T\cos\beta + V} \qquad (2.14)$$

where

T = the bolts or cables acting as the reinforcing forces

JRC = joint roughness coefficient

JCS = joint compressive strength

ϕ_r = residual friction angle

ψ, β = dip angle of plane and the angle between bolting force and weakness

U, V = water force on the joint and tension crack, respectively

This method carries out all possible correlations between the random variables. Using the computer program to select values for each variable to repeats itself until all the nodes in the diagram have been released. The numerical analysis was utilized to comparing the analytical result with the result obtained from the simulation, as the result Monte Carlo simulation is negligible.

Low (1997) presented a closed-form solution to compare several methods of calculating the factor of safety of wedge failure and this solution was generated from equations suggested by Low and Einstein (1992) as follows:

$$FS = \left(a_1 - \frac{b_1 G_{w1}}{S_\gamma} \right) \tan\phi_1 + \left(a_2 - \frac{b_2 G_{w2}}{S_\gamma} \right) \tan\phi_2 + 3b_1 \frac{c_1}{\gamma h} + 3b_2 \frac{c_2}{\gamma h} \tag{2.15}$$

$$a_1 = \frac{\left[\sin\delta_2 \cot\delta_1 - \cos\delta_2 \cos(\beta_1 + \beta_2)\right]}{\sin\psi \sin(\beta_1 + \beta_2)} \tag{2.16a}$$

$$a_2 = \frac{\left[\sin\delta_1 \cot\delta_2 - \cos\delta_1 \cos(\beta_1 + \beta_2)\right]}{\sin\psi \sin(\beta_1 + \beta_2)} \tag{2.16b}$$

$$\begin{aligned} b_1 &= a_0 \sin\beta_2 \sin\delta_2, \\ b_2 &= a_0 \sin\beta_1 \sin\delta_1 \end{aligned} \tag{2.17}$$

$$a_0 = \frac{\sin\psi}{\left[\sin(\beta_1 + \beta_2) \sin\delta_1 \sin\delta_2\right]^2 (\cot\varepsilon - \cot\alpha)} \tag{2.18}$$

$$\tan\varepsilon = \frac{\sin(\beta_1 + \beta_2)}{\sin\beta_1 \cot\delta_2 + \sin\beta_2 \cot\delta_1} \tag{2.19}$$

where

$\beta_1, \beta_2, \delta_1, \delta_2$ are joint orientation angle as show in the figure below

G_{w1}, G_{w2} = normalized water pressure parameters

ϕ_1 , ϕ_2 , c_1 , c_2 = friction angle and cohesion of joints on plane A and plane B, respectively

$S_\gamma = \frac{\gamma}{\gamma_W}$ specific density of rock

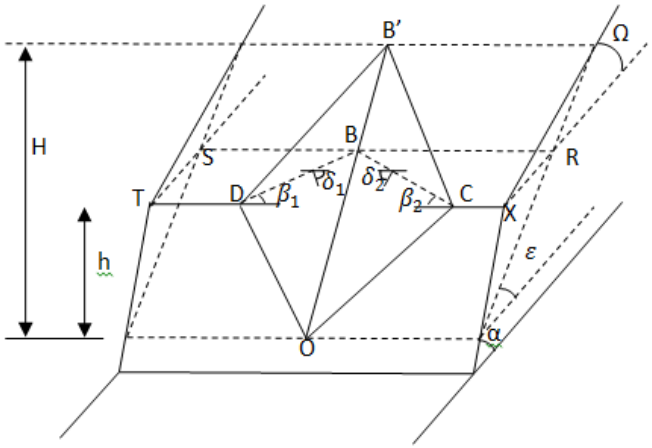

Fig. 2.5. Notations (after Low, 1997)

The Low(1997) proposed six approaches to extend the work as:

- the comparison with Hoek and Bray's (1997) stereographic projection method and vector algebra method to verified closed-form equations
- closed-form equations are also allowed for the wedge sliding along a single face
- a practical spreadsheet method is verified and applied for the calculation of the second-moment reliability index
- the perspective of an expanding ellipsoid is offered as an intuitive way of perceiving the Hasofer-lind index
- the sensitivity information is obtained from simple method
- reliability indices are compared with Monte Carlo simulations

Rodriguez *et al.* (2006) presented system reliability approach to rock slope stability. Their considerations are in two cases include interaction force or without interaction force between blocks A and B separated by a vertical tension crack. They assumed that FS_A greater than 1, this block would be stable, otherwise sliding will be occurred, which presented by Hoek and Bray. In the with interaction force case, they assumed block B is unstable by itself, and block A is stable, but extra load would be acted by block B. The authors also considered two different position of tension crack; one is at slope top, other one is at slope face as show below.

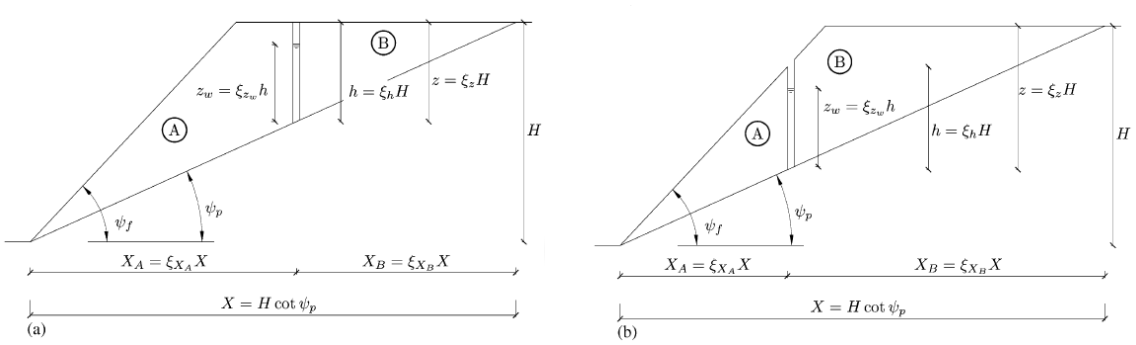

Fig. 2.6. Geometrical definitions of the considered slope stability model (after Rodriguez, 2006). (a) tension crack at slope top; (b) tension crack at slope face

Analyses of these two cases were both based on limiting equilibrium method to compute the factor of safety against sliding of block A and block B. In the reliability analysis, a disjoint cut-set formulation was fulfilled. In addition, four failure modes associated with parallel sub-system. In order to compute the reliability of each parallel sub-system in the disjoint cut-set model, the individual components would be computed at first. The first order reliability method (FORM), linear programming method (LP), Monte Carlo method (MC) and numerical method (NM) to compare each other to point out the characteristic of each method. The authors concluded that FORM provide a simple and computationally efficient approach to present reliability computations, the computation cost of MC is much higher than FORM, and they show a similar result of the probability of failure, LP provide accurate estimations of the system failure probability and flexible way of possible failure probabilities.

2.6 Slope stability analysis based on stereographic method

Rock slope stability is often influenced by structural geological features. The information usually appears in three dimensions with a degree of natural scatter, and for the easy of understanding and use of data in design, an ideal analysis technique has been found that the stereographic projection has ability to show the three dimensional orientation data to be represented in two dimensions.

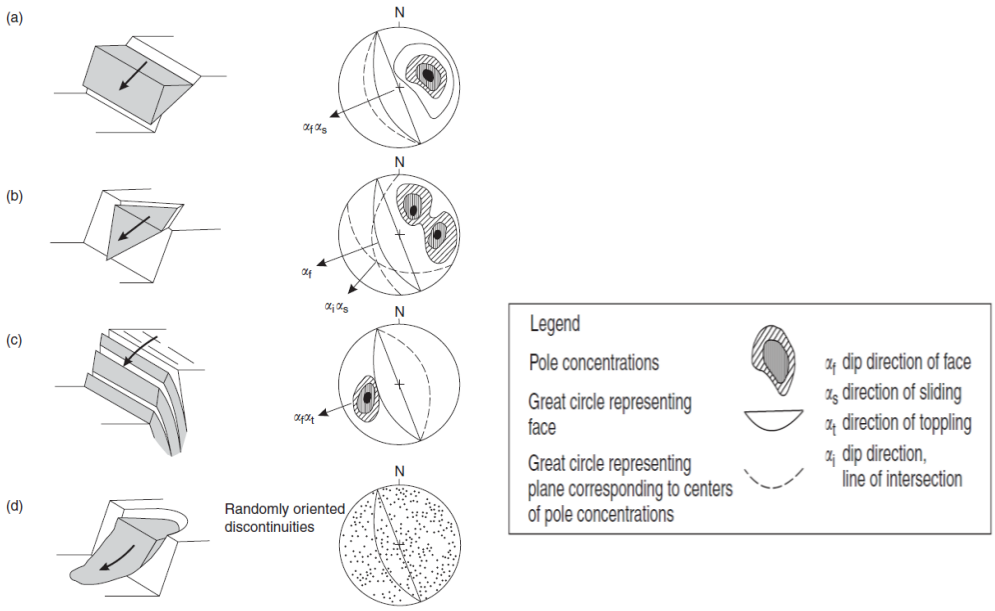

Fig. 2.7. Main types of block failures in slopes, (a) plane failure, (b) wedge failure (c) toppling failure, (d) circular failure (after Hoek and Bray, 1981)

As the figures shown above, the four main types of rock failure were presented by stereonet. This method is useful to identify the potential failure planes by pole concentration. It is also named kinematic analysis.

Hoek (1973) presented kinematic analysis of the factor of safety of rock slope against the wedge failure under water forces and cohesion acting on the sliding surface. As show below:

$$FS = \frac{3}{\gamma_r H}\left(c_A X + c_B Y\right) + \left(A - \frac{\gamma_w}{2\gamma_r} X\right)\tan\phi_A + \left(B - \frac{\gamma_w}{2\gamma_r} Y\right)\tan\phi_B \qquad (2.20)$$

$$X = \frac{\sin\theta_{24}}{\sin\theta_{45}\cos\theta_{2.na}} \tag{2.21}$$

$$Y = \frac{\sin\theta_{13}}{\sin\theta_{35}\cos\theta_{1.nb}} \tag{2.22}$$

$$A = \frac{\cos\psi_a - \cos\psi_b\cos\theta_{na.nb}}{\sin\psi_5\sin^2\theta_{na.nb}} \tag{2.23}$$

$$B = \frac{\cos\psi_b - \cos\psi_a\cos\theta_{na.nb}}{\sin\psi_5\sin^2\theta_{na.nb}} \tag{2.24}$$

where

c_A, c_B = the cohesive strengths on plane A and B, respectively

ϕ_A, ϕ_B = the angle of friction on plane A and B, respectively

γ_w, γ_r = unit weight of the rock and water, respectively

H = slope height

X, Y, A, B = the dimensionless factors, depend upon the geometry of the wedge, as the storeonet show below

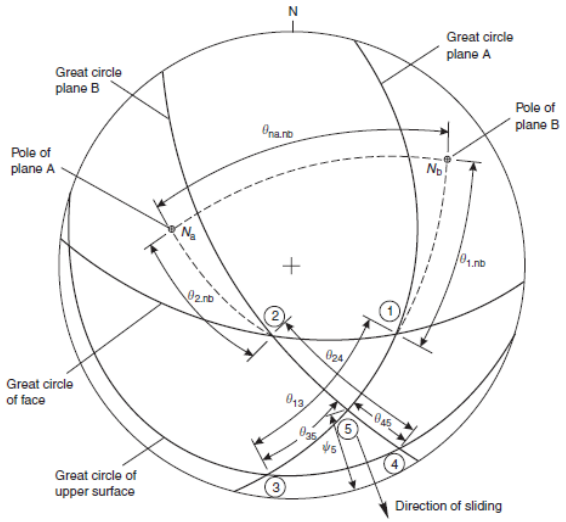

Fig. 2.8. Stereoplot of data required for wedge stability analysis (after Wyllie and Mah, 2005)

2.7 Conclusions

Many researchers have previously studied slope stability, and the methods of slope stability analysis have been presented in 5 sections as static stability analysis, dynamic stability analysis, numerical modeling analysis, reliability analysis and stereographic analysis. But the wedge failure of rock slopes under surcharge and seismic coefficients have not been analysed in detail by any researchers yet. Although, the stabilizing force using anchors has been considered for the plane failure, it has not been considered in wedge failure analysis in the past studies. The limit equilibrium, vector algebra, finite element and closed-form equations methods have been described. Because of the confidence based on many past applications, the limit equilibrium method has been well accepted by the engineers. For the present work, the task is to analyse the slope stability and to derive an expression for the factor of safety against the wedge failure under the surcharge and seismic load with and without anchors for practical applications.

Chapter 3

Analytical Formulation for Wedge Failure Analysis of Rock Slope without Anchors

3.1 General

In this chapter, the derivation of expression for the factor of safety of rock slope against the wedge failure without anchors is presented. The derivation considers most of the factors that may occur in the field conditions under earthquakes and dynamic activities. The surcharge load is also considered to investigate its effect on the factor of safety. Serveral special cases of possible field situations are analysed and discussed in detail.

3.2 General wedge failure conditions and assumptions

Figure 3.1(a) shows a three-dimensional view of a rock slope of height *H* with a tetrahedral wedge block bounded by intersecting joint planes *POM* (Plane 1) and *OQM* (Plane 2), which have *OM* as the line of intersection. The slope is inclined to the horizontal at ψ_f, and *OM* makes an angle of ψ_p with the horizontal. For convenience, the top face has been considered as rectangle $B \times L$. Figure 3.1(b) shows a two-dimensional view of the slope along a vertical section passing through line *OM*. Figure 3.1(c) showns a two-dimensional view of the slope alone a vertical section perpendicular to the line of intersection passing through line YY′, as named section Y-Y′. N_1 and N_2 is the nomal force acting on the plane 1 and plane 2, respectively. Plane 1 is inclinded to vertical at ω_1, and Plane 2 is inclined to vertical at ω_2. The weight of sliding block is W, and horizontal and verticle

seismic forces, k_hW and k_vW, respectively (k_h and k_v are seismic coefficients), are shown to act on the sliding block. A surcharge placed at the top of the slope applies a vertical pressure q. The horizontal and verticle seismic forces also considered on the surcharge, they are $k_hqBD/2$ and $k_vqBD/2$, respectively. The uplift forces due to water pressure on the joint plane 1 and plane 2 are U_1 and U_2, respectively. N is the normal force acting perpendicular to the line of intersection in a plane. s is the shear force. In order to sum of the forces acting on the line of intersection, assume the direction n perpendicular to the line of intersection.

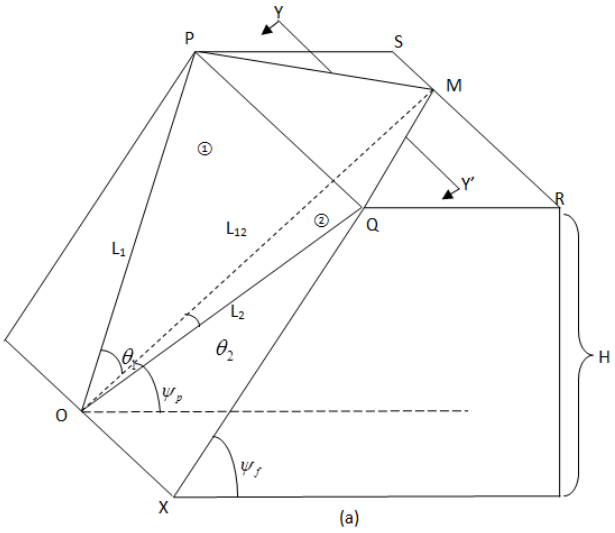

Fig. 3.1. (a) three-dimentional view of the rock slope

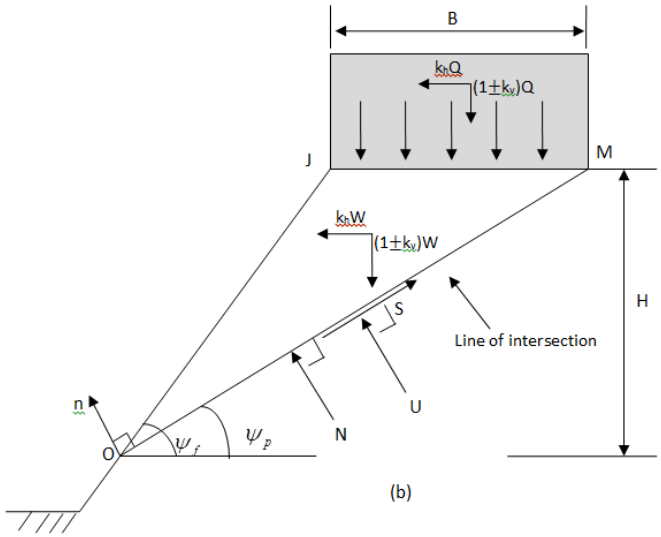

Fig. 3.1. (b) two-dimentional view of the rock slope

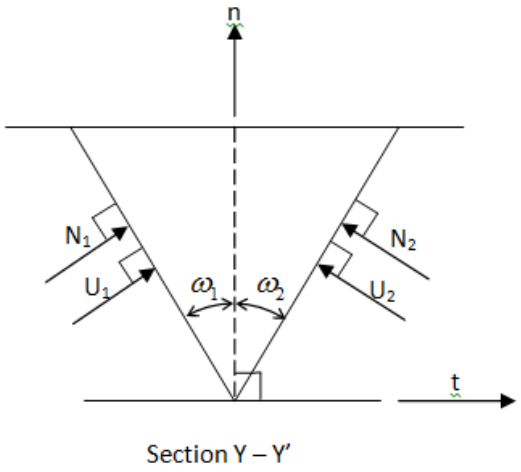

Fig. 3.1. (c) vision of section Y – Y′ of geometry of the rock slope

3.3 Analytical derivation

The factor of safety (FS) of the rock slope is defined as a ratio of the resisting force F_r to the driving force F_i (Kovari and Fritz 1975; Hoek and Bray 1989). Thus

$$FS = \frac{F_r}{F_i} \tag{3.1}$$

It should be noted that F_r is the total force available to resist the block sliding on two wedge planes and F_i is the total force driving the rock wedge to sliding on the two planes.

The Mohr-Coulomb failure criterion (Lambe and Whitman, 1979; Das, 2008) is

$$F_r = cA + (N_1 + N_2)\tan\phi \tag{3.2}$$

where c is the cohesion, A is the total base area OPM and OQM, and N_1, N_2 are the normal forces acting on the failure plane 1 and plane 2, and ϕ is the angle of shearing resistance of the material at the failure plane.

As Fig.3.1 (b) shows, sum of all the forces acting on the slope along the normal to the line of intersection is

$$\sum F_n = W\left(\cos\psi_p - k_h \sin\psi_p \pm k_v \cos\psi_p\right) + Q\cos\psi_p - k_h Q\sin\psi_p \pm k_v Q\cos\psi_p - N = 0 \tag{3.3}$$

Sum all the forces acting on the slope along the t direction as shown in Fig. 3.1 (c) is

$$\sum F_t = (N_1 + U_1)\cos\omega_1 - (N_2 + U_2)\cos\omega_2 = 0 \tag{3.4}$$

N is the normal force acting on the line of intersection of the slope (Fig.3.1 (c)) as given

$$N = (N_1 + U_1)\sin\omega_1 + (N_2 + U_2)\sin\omega_2 \tag{3.5}$$

Sum of normal forces on plane 1 and plane 2 can be obtained from simultaneous equations (3.3) and (3.4) (the details are given in the appendix) as

$$N_1 + N_2 = \left[W\left(\cos\psi_p - k_h \sin\psi_p \pm k_v \cos\psi_p\right) + Q\cos\psi_p - k_h Q\sin\psi_p \pm k_v Q\cos\psi_p\right]\lambda - U \tag{3.6}$$

Thus the total resisting forces is given as:

$$F_r = cA + \left\{\left[W\left(\cos\psi_p - k_h \sin\psi_p \pm k_v \cos\psi_p\right) + Q\cos\psi_p - k_h Q\sin\psi_p \pm k_v Q\cos\psi_p\right]\lambda - U\right\}\tan\phi \tag{3.7}$$

The total driving force is calculated as:

$$F_i = W\sin\psi_p + Wk_h\cos\psi_p \pm Wk_v\sin\psi_p + Q\sin\psi_p + k_h Q\cos\psi_p \pm k_v Q\sin\psi_p$$

$$= (W + Q)\left[(1 \pm k_v)\sin\psi_p + k_h\cos\psi_p\right] \tag{3.8}$$

From equations (3.7) and (3.8), the factor of safety is

$$FS = \frac{F_r}{F_i} = \frac{cA + \left\{\left[W\left(\cos\psi_p - k_h \sin\psi_p \pm k_v \cos\psi_p\right) + Q\cos\psi_p - k_h Q\sin\psi_p \pm k_v Q\cos\psi_p\right]\lambda - U\right\}\tan\phi}{(W + Q)\left[(1 \pm k_v)\sin\psi_p + k_h\cos\psi_p\right]} \tag{3.9}$$

The parameters $A, W, \sigma_{sur}, \lambda$ and U are obtained as follows

$$A = A_1 + A_2 = \frac{L_1 L_{12}\sin\theta_1}{2} + \frac{L_2 L_{12}\sin\theta_2}{2} = \frac{H(L_1\sin\theta_1 + L_2\sin\theta_2)}{2\sin\psi_p} \tag{3.10}$$

where A is the total connect area between failure plane and rock slope, θ_1 is the angle between L_1 and L_{12}, and θ_2 is the angle between L_2 and L_{12}.

The weight of the sliding rock mass block $OREP$ is

$$W = \gamma V = \gamma H \frac{BD}{6} \tag{3.11}$$

where γ is the unit weight of rock mass.

The surcharge loading on the wedge block Q ($PQRS$ is a rectangular shape) is

$$Q = \frac{qBD}{2} \tag{3.12}$$

with

$$B = \frac{H}{\tan\psi_p} - \frac{H}{\tan\psi_f} = H(\cot\psi_p - \cot\psi_f) \tag{3.13}$$

where B represent JM in Fig. 3.1 (b).

λ is called the wedge factor by Kovari and Fritz (1975) as given below:

$$\lambda = \frac{\cos\omega_1 + \cos\omega_2}{\sin(\omega_1 + \omega_2)} \tag{3.14}$$

where ω_1, ω_2 are the angles between the surface A and the vertical and the angle between the surface B and the vertical, respectively.

Uplift force on the sliding block due to water pressure on failure planes 1 and 2 is

$$U = U_1 + U_2 = \frac{\gamma_w H}{6} A_u + \frac{\gamma_w H}{6} A_u = \frac{\gamma_w H}{3} A_u \tag{3.15}$$

where γ_w is the unit weight of water.

The cross-sectional area (OJM) of wedge block is

$$A_u = \frac{BH}{2} \tag{3.16}$$

Thus the equation of FS becomes

$$FS = \frac{F_r}{F_i} = \frac{c\dfrac{H(L_1\sin\theta_1 + L_2\sin\theta_2)}{2\sin\psi_p} + \left\{\left[\begin{array}{l}\gamma H\dfrac{BD}{6}\left(\cos\psi_p - k_h\sin\psi_p \pm k_v\cos\psi_p\right)\\ +\dfrac{qBD}{2}\cos\psi_p - k_h\dfrac{qBD}{2}\sin\psi_p \pm k_v\dfrac{qBD}{2}\cos\psi_p\end{array}\right]\dfrac{\cos\omega_1+\cos\omega_2}{\sin(\omega_1+\omega_2)} - \dfrac{\gamma_w BH^2}{6}\right\}\tan\phi}{\left(\gamma H\dfrac{BD}{6} + \dfrac{qBD}{2}\right)\left[(1\pm k_v)\sin\psi_p + k_h\cos\psi_p\right]} \quad (3.17)$$

$$FS = \frac{F_r}{F_i} = \frac{c\dfrac{H(L_1\sin\theta_1 + L_2\sin\theta_2)}{2\sin\psi_p} + \left\{\left[\dfrac{BD}{6}\left(\begin{array}{l}\cos\psi_p - k_h\sin\psi_p\\ \pm k_v\cos\psi_p\end{array}\right)(\gamma H + 3q)\right]\dfrac{\cos\omega_1+\cos\omega_2}{\sin(\omega_1+\omega_2)} - \dfrac{\gamma_w BH^2}{6}\right\}\tan\phi}{\dfrac{1}{6}BD(\gamma H + 3q)\left[(1\pm k_v)\sin\psi_p + k_h\cos\psi_p\right]} \quad (3.18)$$

Dividing by γH^3, the equation becomes

$$FS = \frac{F_r}{F_i} = \frac{\dfrac{c(\frac{L_1}{H}\sin\theta_1 + \frac{L_2}{H}\sin\theta_2)}{2\gamma H\sin\psi_p} + \left\{\begin{array}{l}\left[\dfrac{1}{6}\dfrac{D}{H}(\cot\psi_p - \cot\psi_f)\left(\cos\psi_p - k_h\sin\psi_p \pm k_v\cos\psi_p\right)(1+3\dfrac{q}{\gamma H})\right]\\ \dfrac{\cos\omega_1+\cos\omega_2}{\sin(\omega_1+\omega_2)} - \dfrac{\gamma_w}{6\gamma}(\cot\psi_p - \cot\psi_f)\end{array}\right\}\tan\phi}{\dfrac{1}{6}\dfrac{D}{H}(\cot\psi_p - \cot\psi_f)\left(1+\dfrac{3q}{\gamma H}\right)\left[(1\pm k_v)\sin\psi_p + k_h\cos\psi_p\right]} \quad (3.19)$$

In order to find an easy way to work on the parametric analysis, the following nondimensional parameters are defined:

$$c^* = \frac{c}{\gamma H}, \gamma^* = \frac{\gamma}{\gamma_w}, q^* = \frac{q}{\gamma H}, L_1{}^* = \frac{L_1}{H}, L_2{}^* = \frac{L_2}{H}, D^* = \frac{D}{H}.$$

$$FS = \frac{F_r}{F_i} = \frac{\dfrac{c^*(L_1{}^*\sin\theta_1 + L_2{}^*\sin\theta_2)}{2\sin\psi_p} + \left\{\begin{array}{l}\left[\dfrac{1}{6}D^*(\cot\psi_p - \cot\psi_f)\left(\cos\psi_p - k_h\sin\psi_p \pm k_v\cos\psi_p\right)(1+3q^*)\right]\\ \dfrac{\cos\omega_1+\cos\omega_2}{\sin(\omega_1+\omega_2)} - \dfrac{(\cot\psi_p - \cot\psi_f)}{6\gamma^*}\end{array}\right\}\tan\phi}{\dfrac{1}{6}D^*(\cot\psi_p - \cot\psi_f)(1+3q^*)\left[(1\pm k_v)\sin\psi_p + k_h\cos\psi_p\right]} \quad (3.20)$$

3.4 Special cases

Case 1: The joint material is cohesionless, and there are no surcharge, seismic forces and water force, that is $c^* = 0, \phi \neq 0, q^* = 0, k_h = 0, k_v = 0$ and $U = \dfrac{(\cot\psi_p - \cot\psi_f)}{6\gamma^*} = 0$

Equation (3.20) becomes

$$FS = \frac{\lambda \tan\phi}{\tan\psi_p} \tag{3.21}$$

Case 2: The joint material is cohesive and there are no seismic forces and water in the tension crack, that is, $c^* = 0, \phi \neq 0, q^* \neq 0, k_h = 0, k_v = 0$ and $U = 0$.

Equation (3.20) becomes

$$FS = \frac{F_r}{F_i}$$
$$= \frac{\left\{[\frac{1}{6}D^* \cos\psi_p(\cot\psi_p - \cot\psi_f)(1+3q^*)]\dfrac{\cos\omega_1 + \cos\omega_2}{\sin(\omega_1+\omega_2)}\right\}\tan\phi}{\frac{1}{6}D^* \sin\psi_p(\cot\psi_p - \cot\psi_f)(1+3q^*)} = \frac{\lambda\tan\phi}{\tan\psi_p} \tag{3.22}$$

Case 3: The joint material is c - ϕ material, and there are no seismic forces and water in the tension crack, that is, $c^* \neq 0, \phi = 0, q^* \neq 0, k_h = 0, k_v = 0$ and $U = 0$.

Equation (3.20) becomes

$$FS = \frac{F_r}{F_i} = \frac{\dfrac{c^*(L_1{}^* \sin\theta_1 + L_2{}^* \sin\theta_2)}{2\sin\psi_p}}{\frac{1}{6}D^* \sin\psi_p(\cot\psi_p - \cot\psi_f)(1+3q^*)} \tag{3.23}$$

Case 4: The joint material is c - ϕ material, and there are no seismic forces, that is, $c^* \neq 0, \phi \neq 0, q^* \neq 0, k_h = 0, k_v = 0$ and $U = 0$.

Equation (3.20) becomes

$$FS = \frac{F_r}{F_i} = \frac{\dfrac{c^*(L_1^* \sin\theta_1 + L_2^* \sin\theta_2)}{2\sin\psi_p} + \left\{\left[\left[\dfrac{1}{6} D^* \cos\psi_p (\cot\psi_p - \cot\psi_f)(1+3q^*)\right]\dfrac{\cos\omega_1 + \cos\omega_2}{\sin(\omega_1+\omega_2)}\right\}\tan\phi}{\dfrac{1}{6} D^* \sin\psi_p (\cot\psi_p - \cot\psi_f)(1+3q^*)} \tag{3.24}$$

Case 5: The joint material is c - ϕ material, and there are only horizontal seismic forces, that is, $c^* \neq 0, \phi \neq 0, q^* \neq 0, k_h = 0, k_v = 0,$ and $U \neq 0$.

Equation (3.20) becomes

$$FS = \frac{F_r}{F_i}$$

$$= \frac{\dfrac{c^*(L_1^* \sin\theta_1 + L_2^* \sin\theta_2)}{2\sin\psi_p} + \left\{\begin{array}{l}\left[\left[\dfrac{1}{6} D^* \cos\psi_p (\cot\psi_p - \cot\psi_f)(1+3q^*)\right]\dfrac{\cos\omega_1 + \cos\omega_2}{\sin(\omega_1+\omega_2)}\right] \\ -\dfrac{(\cot\psi_p - \cot\psi_f)}{6\gamma *}\end{array}\right\}\tan\phi}{\dfrac{1}{6} D^* \sin\psi_p (\cot\psi_p - \cot\psi_f)(1+3q^*)} \tag{3.25}$$

Case 6: The joint material is c - ϕ material, and there are only horizontal seismic forces, that is, $c^* \neq 0, \phi \neq 0, q^* \neq 0, T^* \neq 0, k_h \neq 0, k_v = 0,$ and $U \neq 0$.

Equation (3.20) becomes

$$FS = \frac{F_r}{F_i}$$

$$= \frac{\dfrac{c^*(L_1^* \sin\theta_1 + L_2^* \sin\theta_2)}{2\sin\psi_p} + \left\{\begin{array}{l}\left[\dfrac{1}{6} D^* (\cot\psi_p - \cot\psi_f)(\cos\psi_p - k_h \sin\psi_p)(1+3q^*)\right] \\ \dfrac{\cos\omega_1 + \cos\omega_2}{\sin(\omega_1+\omega_2)} - \dfrac{(\cot\psi_p - \cot\psi_f)}{6\gamma^*}\end{array}\right\}\tan\phi}{\dfrac{1}{6} D^* (\cot\psi_p - \cot\psi_f)(1+3q^*)(\sin\psi_p + k_h \cos\psi_p)} \tag{3.26}$$

3.5 Variation of factor of safety for different special cases

Figure 3.2 shows the variation of factor of safety of the rock slope with angle of shearing resistance of the joint material for several possible field situations as above case 1 to case 6, considering a particular set of governing parameters in their non-dimensional form as: $\psi_f = 50°$, $\psi_p = 35°$, $c^* = 0.08$, $D^* = 0.6$, $\gamma^* = 2.5$, $L_1^* = L_2^* = 1.4$, $k_h = 0.1$, $k_v = 0.05$, $q^* = 0.25$, , $\theta_1 = \theta_2 = 25°$ and $\omega_1 = \omega_2 = 30°$. It is noted that the factor of safety of rock slope increases with an increase in ϕ, the rate of increasing of factor of safety is higher with equation (3.21). As expected, the cohesion is increasing factor of safety for any ϕ. From equations (3.25) and (3.26) in the line chart, it can be seen that the horizontal seismic force decreases the factor of safety. For the vertical seismic force, the upward direction of seismic force does not affect the factor of safety for this type of condition. The water force and surcharge both are the destabilizing forces for rock slope, and they are decreasing the factor of safety of the rock slope.

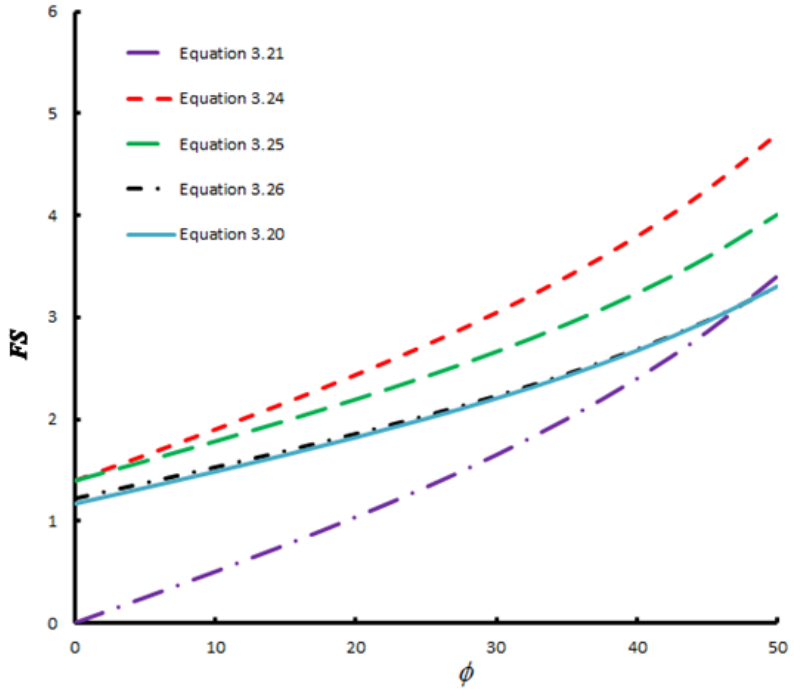

Fig. 3.2. Variation of factor of safety of the rock slope with angle of shearing resistance of the joint material for several possible field situations

Figure 3.3 shows variation of factor of safety of the rock slope with cohesion of the joint material for several possible field situations as above case 1 to case 6, considering a particular set of governing parameters in their nondimensional form as $\psi_f = 50°$, $\psi_p = 35°$, $D^* = 0.6$, $\gamma^* = 2.5$, $L_1^* = L_2^* = 1.4$, $k_h = 0.1$, $k_v = 0.05$, $q^* = 0.25$, $\theta_1 = \theta_2 = 25°$ and $\omega_1 = \omega_2 = 30°$. It is observed that the factor of safety increases almost linearly with an increase in cohesion. It is also noted that the factor of safety reached a highest value when water force and seismic force is equal to zero. The factor of safety become the lowest value when ϕ is equal to zero. The vertical seismic force slightly affects the factor of safety.

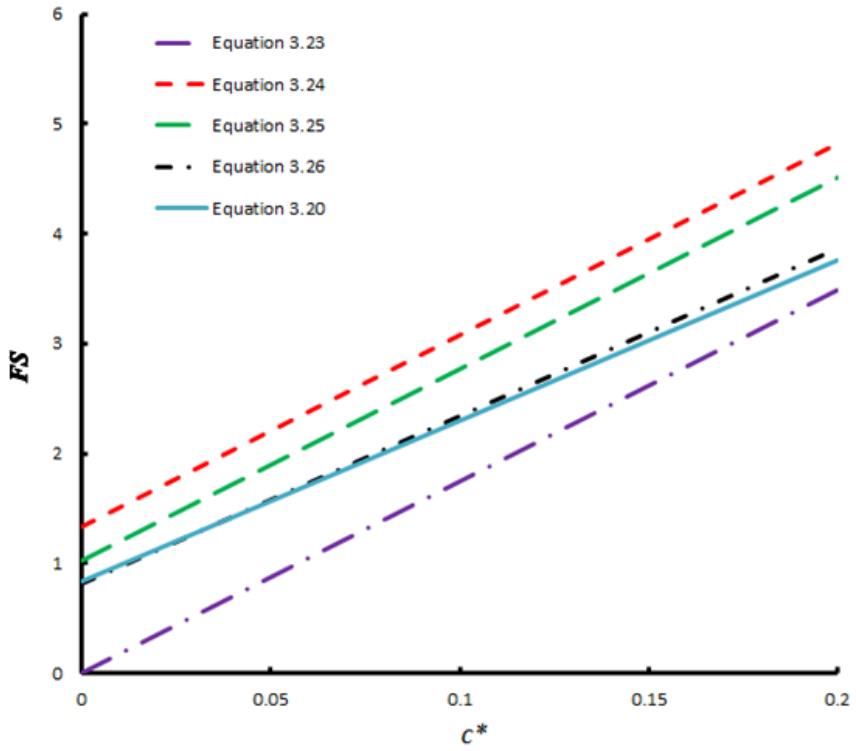

Fig. 3.3. Variation of factor of safety of the rock slope with cohesion of the joint material for several possible field situations

3.6 Conclusions

In this chapter, an expression for the factor of safety against the wedge failure under surcharge and seismic force is derived as equation (3.20), with most forces occurring in the real field. Six special cases are presented for several possible field situations. It was observed that the factor of safety of the rock slope increases with an increase in both angle of shearing resistance and cohesion of the joint material. The value of factor of safety of equation (3.24) is always greater than others, because the water force and surcharge both are destabilizing forces for the rock slope. The horizontal seismic force decreases the factor of safety, whereas the vertical seismic force slightly affects the factor of safety.

Chapter 4

Parametric Study for Wedge Failure Analysis of Rock Slope without Anchors

4.1 General

In this chapter, the parametric study is carried out for analysis of effect of governing parameters on the factor of safety which has been discussed in detail in Chapter 3. This study would focus on the effect on the factor of safety by increasing the surcharge for different governing parameters. There can be several slope geometries, and also a wide variation in joint and rock properties may take place in real field situations. For illustrative purpose, the parameters are assumed to be in the engineers' practical data range as presented in the following section.

4.2 Range of parameters

The parametric study has been made to investigate the effects of surcharge on the stability of rock slope. The considered ranges of parametera as shown below:

Angle of inclination of the failure plane to the horizontal	ψ_p : $30° - 40°$
Angle of inclination of the slope face to the horizontal	ψ_f : $40° - 60°$
Cohesion	c^* : 0 – 0.16
Angle of shearing resistance	ϕ: $20° - 40°$
Unit weight of rock	γ^*: 2.5– 2.9
Surcharge pressure	q^*: 0 – 2.4

Horizontal seismic coefficient	k_h : 0 – 0.3
Vertical seismic coefficient	k_v : -0.15 – 0.15
Dips of planes 1 and 2	ω_1, ω_2 : $20^\circ - 30^\circ$

4.3 Effect of stabilizing force for factor of safety with different value of governing parameters

Figure 4.1 shows the variation of the factor of safety (FS) with surcharge q^* for different dimensionless values of cohesion, c^* = 0.00, 0.04, 0.08, 0.12 and 0.16; considering specific value of governing parameters in their nondimensional form as: $\psi_f = 50°$, $\psi_p = 35°$, $\phi = 25°$, $D^* = 0.6$, $\gamma^* = 2.5$, $L_1^* = L_2^* = 1.4$, $k_h = 0.1$, $k_v = 0.05$, $\theta_1 = \theta_2 = 25°$ and $\omega_1 = \omega_2 = 30^\circ$. It is observed that the FS declines sharply from 4.7 to 2.6, 3.7 to 2.3 and 2.7 to 1.7 (with c^* = 0.16, 0.12 and 0.08) as q^* increases from 0 to 0.5. The FS is reduced moderately as q^* increases from 0.5 to 1.5; as q^* increases more than 1.5, FS does not change much. However, once c^* = 0, the factor of safety shows an increasing trend, from 0.6 to 1.1 as q* increases from 0 to 2.5. In particularly, the FS is close to a stable level of 1.4 when c^* = 0.04 with increase in q^* greater than 0.5 and where the surcharge has no impact. The factor of safety equals to 1 that is critical value, so a horizontal line at FS = 1 has been drawn as a mark between the stable part above the line and the unstable part below the line. For this case the curve of c^* = 0 always in the unstable part which is FS < 1. As expected, the greater the cohesion, the greater the factor of safety. As the figure shows the FS increases significantly with an increase in cohesion.

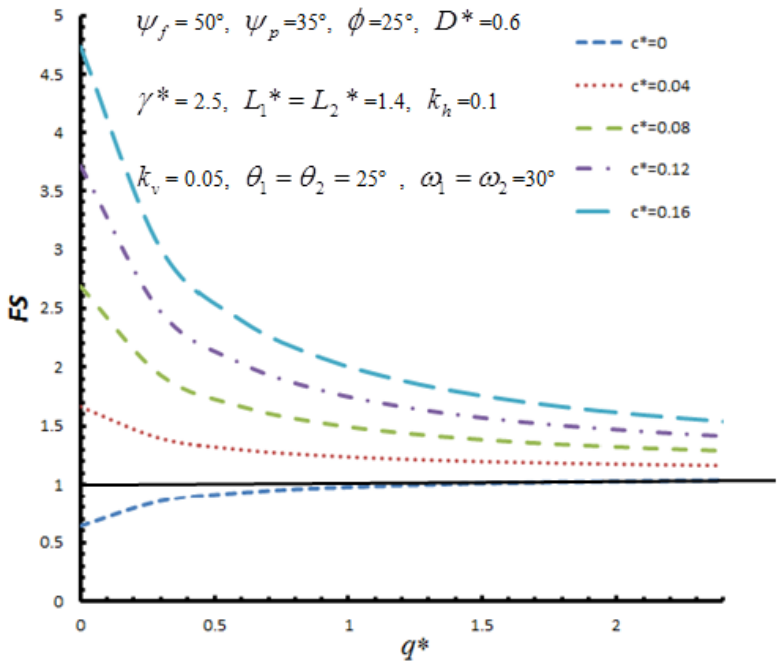

Fig. 4.1. Variation of factor of safety (FS) with surcharge (q^*) for different values of c^*.

Figure 4.2 shows the variation of the factor of safety (FS) with surcharge q^* for different value of angle of shearing resistance, ϕ =20°, 25°, 30°, 35° and 40°; considering specific value of governing parameters in their nondimensional form as: ψ_f = 50°, ψ_p = 35°, c^* =0.08, D^* = 0.6, γ^* = 2.5, $L_1^* = L_2^* = 1.4$, k_h = 0.1, k_v = 0.05, $\theta_1 = \theta_2$ = 25° and $\omega_1 = \omega_2 = 30^\circ$. It is illustrated that there is a positive relationship between the factor of safety (FS) and the angle of shearing resistance, but the FS decreases as the surcharge increases. When the surcharge increase from 0 to 0.5, the rate of decrease is much higher than the value of surcharge is greater than 0.5. The curve with a lower angle of shearing resistance showed this significant trend more clearly. For example, for ϕ = 25°, the FS decreases from 2.7 to 1.7 with the surcharge increasing from 0 to 0.5; whereas the increase of more than 0.5 in surcharge does not affect the FS a lot, the FS decreases from 1.7 (with q^* = 0.5) to 1.4 (with q^* = 2.5). From the chart, it is also found that the FS decreases close to 1

(with ϕ =20°) when the increase in surcharge gets to 2.5.

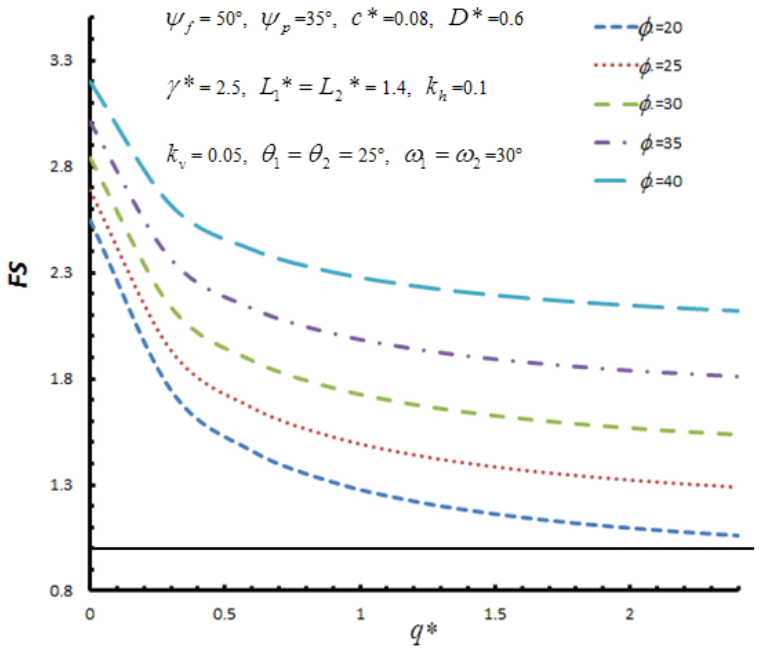

Fig. 4.2. Variation of factor of safety (FS) with surcharge (q^*) for different values of angle of shearing resistance (ϕ)

Figure 4.3 shows the variation of the factor of safety (FS) with surcharge q^* for different value of unit weight of rock, γ^* = 2.5, 2.6, 2.7, 2.8, 2.9; considering specific value of governing parameters in their nondimensional form as: ψ_f = 50°, ψ_p = 35°, c^* = 0.08, D^* = 0.6, ϕ = 25°, γ^* = 2.5, $L_1^* = L_2^* = 1.4$, k_h = 0.1, k_v = 0.05, $\theta_1 = \theta_2$ = 25° and $\omega_1 = \omega_2 = 30^\circ$. It is noted that the factor of safety goes down with an increase in surcharge and decreases sharply, when the surcharge is between 0 and 0.5, the FS decreases at a relative higher rate for all practical values of γ^*. For example, the FS increases from 2.76 to 1.72 with γ^* = 2.9. The FS decreases moderately as the surcharge increases over 0.5. For example, FS decreases by 0.2 from 1.72 to 1.52 with γ^* = 2.9 as q^* increases from 0.5 to 1.0. From Figure 4, a clear trend is illustrated that the factor of safety has not

been affected much by different unit weights of rock. The reason is that, the increase in the self-weight of rock gives rise to two components of the weight force. One acts on the sliding surface as a normal force, thus increasing the sliding resistance. The other one along the sliding direction acts as a driving force. Two forces go in an opposite direction, so they cancel each other such that the magnitude of γ^* has little effect.

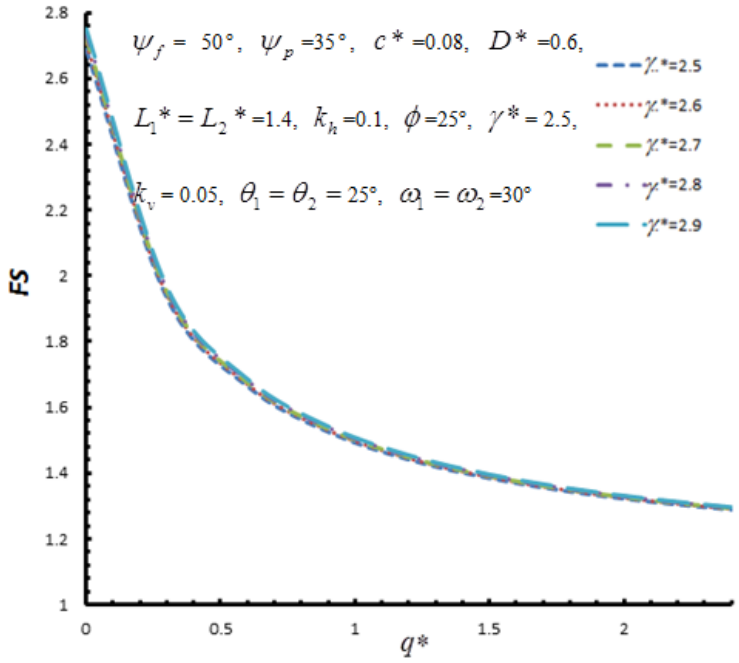

Fig. 4.3. Variation of factor of safety (FS)with surcharge (q^*) for different values of unit weight of rock (γ^*)

Figure 4.4 shows the variation of the factor of safety (FS) with surcharge q^* for different values of angle of inclination of the slope face to horizontal, ψ_f = 40°, 45°, 50°, 55° and 60°; considering specific value of governing parameters in their nondimensional form as: ψ_p = 35°, γ^* = 2.5, c^* = 0.08, D^* = 0.6, ϕ = 25°, $L_1^* = L_2^* = 1.4$, k_h = 0.1, k_v = 0.05, $\theta_1 = \theta_2$ = 25° and $\omega_1 = \omega_2 = 30^\circ$. It is observed that the factor of safety decreases at a higher rate for the lower value of surcharge, especially, between 0 and 0.5. For example, the *FS* decreased by about 48%, from 5.8 to 3.0 with ψ_p =

40°. It is also noted that for the inclination of the slope face to the horizontal greater than 50 degrees, the FS almost stays at the same value when a surcharge increase greater than 1, that is, the *FS* is not affected much by increasing the surcharge on steep slopes.

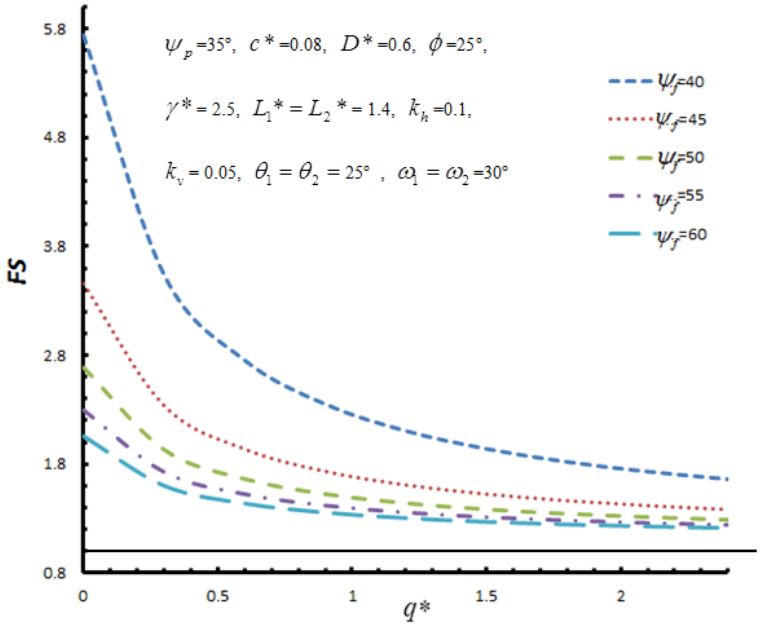

Fig. 4.4. Variation of factor of safety (FS) with surcharge (q^*) for different values of angle of inclination of the slope face to the horizontal (ψ_f)

Figure 4.5 shows the variation of the factor of safety (FS) with surcharge q^* for different values of angle of inclination of the failure plane to the horizontal, ψ_p = 30°, 33°, 35°, 37° and 40°; considering specific value of governing parameters in their nondimensional form as: ψ_f = 50°, γ^* = 2.5, c^* = 0.08, D^* = 0.6, ϕ = 25°, $L_1^* = L_2^* = 1.4$, k_h = 0.1, k_v = 0.05, $\theta_1 = \theta_2$ = 25° and $\omega_1 = \omega_2 = 30^\circ$. It is illustrated that the FS decreases with the increase in surcharge. As surcharge increases from 0 to 0.5, the rate of decrease is much higher than that when the value of surcharge is greater than 0.5. For example, the factor of safety decreases from 3.35 to 2.0 with ψ_p = 40° as the surcharge increases from 0 to 0.5; whereas when an increase in surcharge is more than 0.5, the rate of

decrease of factor of safety goes down, it decreases form 2.0 (with q^* = 0.5) to 1.6 (with q^* = 1). It is also observed that the highest value of the FS with the biggest angle of failure plane to the horizontal when there is no surcharge, while the highest value of the FS with smallest angle of failure plane to the horizontal when there is a high surcharge (greater than 1.3).

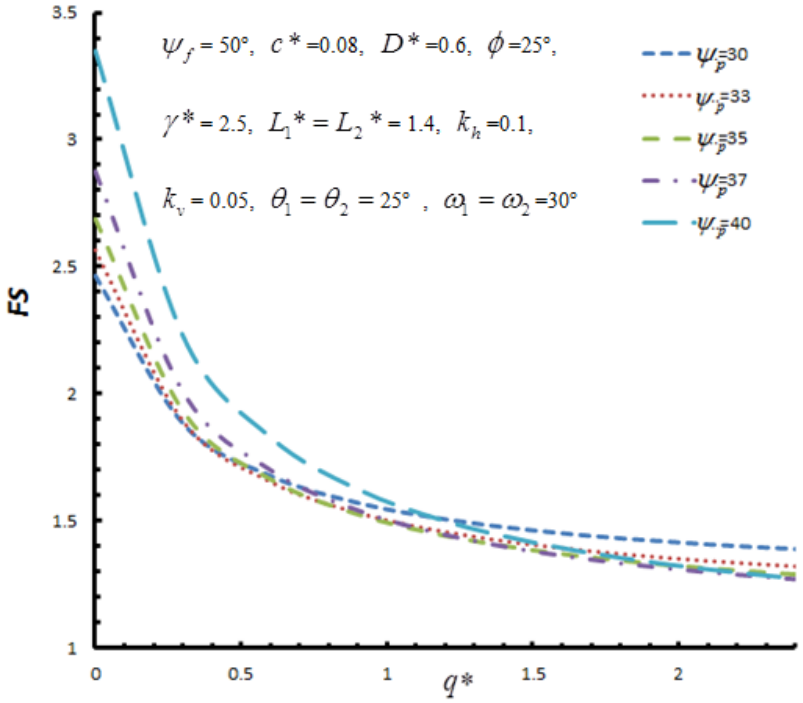

Fig. 4.5. Variation of factor of safety (FS) with surcharge (q^*) for different values of angle of inclination of the failure plane to the horizontal (ψ_p)

Figure 4.6 shows the variation of the factor of safety (FS) with surcharge q^* for different value of horizontal seismic force, k_h = 0, 0.05, 0.1, 0.15, 0.2, 0.25 and 0.3; considering specific value of governing parameters in their nondimensional form as: ψ_f = 50°, ψ_p = 35°, γ^* = 2.5, c^* = 0.08, D^* = 0.6, ϕ = 25°, $L_1^* = L_2^* = 1.4$, k_v = 0.05, $\theta_1 = \theta_2$ = 25° and $\omega_1 = \omega_2 = 30^\circ$. It is observed that the greater value of factor of safety

comes with smaller value of horizontal seismic force, but FS decreases as the surcharge increases and the FS decreasing trend is almost the same with different k_h. when the surcharge increases from 0 to 0.5, the rate of decrease is much higher than that for the value of surcharge greater than 0.5. For example, for k_h = 0.15, the factor of safety decreases from 2.5 to 1.6 when a surcharge increases from 0 to 0.5, whereas when the increase in surcharge is more than 0.5, the decrease of the FS slows down. For example, it decreases from 1.6 (with q^* = 0.5) to 1.4 (with q^* = 1.0). Once, k_h is greater than 0.25, the FS decreases to an unstable region with an increase in surcharge greater than 2.

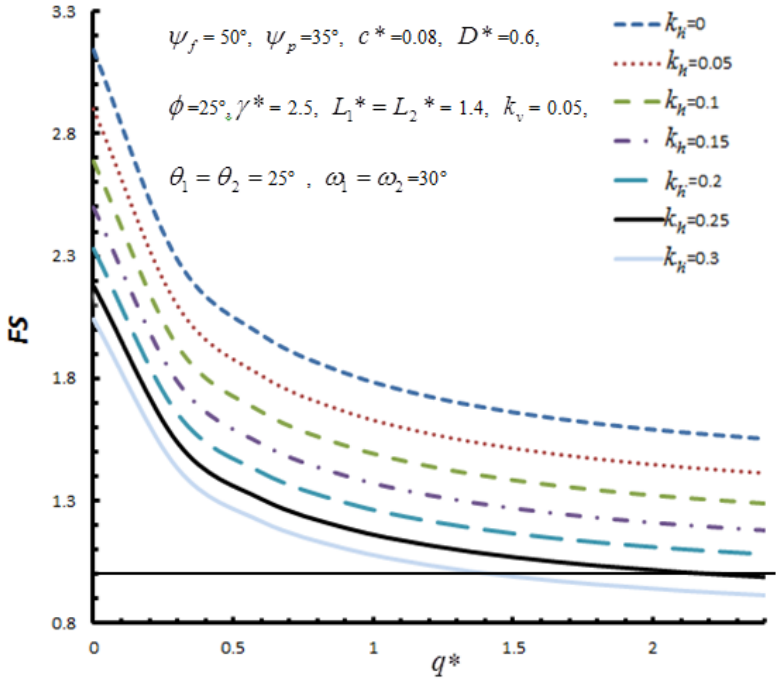

Fig. 4.6. Variation of factor of safety (FS) with surcharge (q^*) for different values of horizontal seismic force (k_h).

Figure 4.7 shows the variation of the factor of safety (FS) with surcharge q^* for different value of horizontal seismic force, k_v = -0.15, -0.1, -0.05, 0, 0.05, 0.1 and 0.15; considering specific value of governing parameters in their nondimensional form as: ψ_f = 50°, ψ_p = 35°, γ^* = 2.5, c^* = 0.08, D^* = 0.6, ϕ = 25°, $L_1^* = L_2^*$ = 1.4, k_h = 0.1,

$\theta_1 = \theta_2 =$ 25° and $\omega_1 = \omega_2 = 30^\circ$. It is noted that the factor of safety goes down with an increase in surcharge and decreases sharply as the surcharge is between 0 and 0.5, from 2.96 to 1.8 with k_v = -0.15. The factor of safety decreases moderately as the increase in surcharge is more than 0.5. For example, FS decreases by 0.24 from 1.8 to 1.56 with k_v = -0.15 as q^* increases from 0.5 to 1.0. A key point is that all values on the curve intersect at a point at q^* = 1.9, and, after this point, all values of FS on the curve reverse their orders of impact, for example, the highest value of FS with k_v = -0.15 becomes the lowest value, and the lowest value of FS with k_v = 0.15 turns to the highest value.

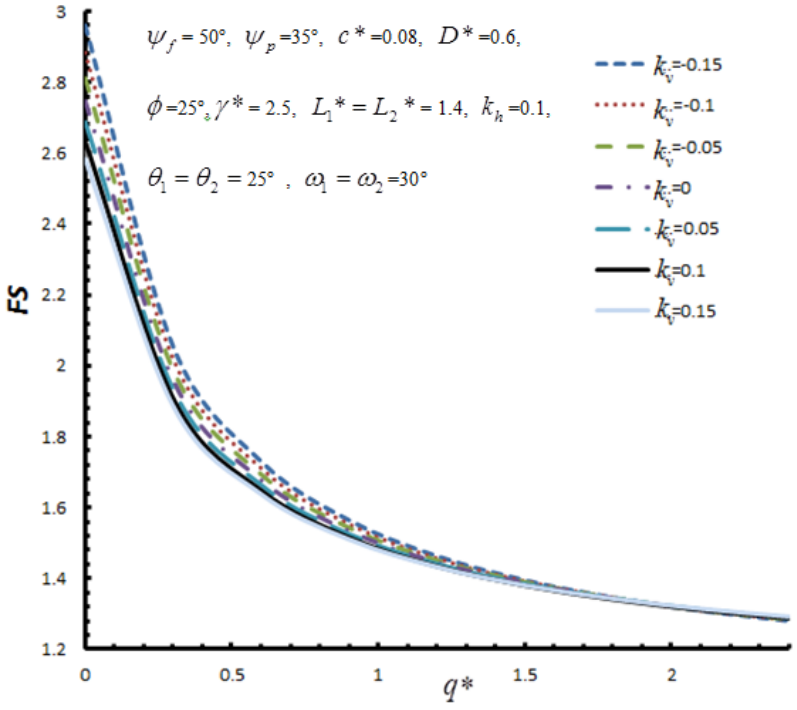

Fig. 4.7. Variation of factor of safety (FS) with surcharge (q^*) for different values of vertical seismic force (k_v).

4.4 Conclusions

The parametric study, presented in the previous section is used to investigate the effect of

surcharge on the stability of the rock slopes. The parametric study reveals that the factor of safety (FS) of rock slope decreases with an increase in surcharge. Lower value of surcharge makes the factor of safety decreases relatively faster. The FS is relatively higher with greater value of cohesion and angle of shearing resistance (ϕ) for any surcharge. The FS shows a rapid decreasing trend with an increase in surcharge for greater value of cohesion (c^*). Whereas, the FS decreases in almost the same trend with an increase in surcharge for any angle of shearing resistance (ϕ).

The FS increases with an increase in unit weight of rock, but the FS is not much affected by variation in unit weight of rock (γ^*) for any value of surcharge. The FS increases with a decrease in the values of angle of inclination of the slope face to the horizontal (ψ_f) for any surcharge value. Whereas, the FS increases with an increase in the values of angle of inclination of the failure plane to the horizontal (ψ_p) for lower values of surcharge (less than 1.5); it increases with a decrease in ψ_p for greater value of surcharge (greater than 1.5). The different directions of seismic force affect the FS differently. The FS increases with a decrease in horizontal seismic force for any value of surcharge; however, the FS increases with a decrease in vertical seismic force for a value of surcharge less than 1.5, after this point, all values of FS on the curve reverse their orders of impact, and the FS increases with an increase in the value of vertical seismic force.

Chapter 5

Analytical Formulation for Wedge Failure Analysis of Anchored Rock Slope

5.1 General

In this chapter, based on the previous study in Chapter 3, this study adds a stabilizing force T as the anchor force for rock slope system to analyse the derivation of expression for the factor of safety. However, there are different types of anchored system for the rock slope against the wedge failure. Because of the wedge block has two planes, the anchors would stabilize it by going through planes or going through intersection line of planes, and the angle between anchors and planes also need to be considered. Three different anchored systems of rock slope have been compared to find out the largest stabilizing force against the wedge failure. The analytical formulation is based on the results of the comparison section to derive an expression for factor of safety of an anchored rock slope against wedge failure. Serveral special cases of possible field situations are analysed and discussed in detail.

5.2 Different anchored systems for the rock slope

5.2.1 Anchored system #1

As shown in Fig. 5.1 N_1 and N_2 are the normal force acting on the plane 1 and plane 2, respectively. Plane 1 is inclinded to vertical at ω_1, and plane 2 is inclined to vertical at ω_2. Anchors are perpendicular across the slope face to both planes for the stabilizing force T_1 and T_2.

The N is the normal force acting on the line of intersection of the slope, given as

$$N = (N_1 + U_1 - T_1 \sin\omega_1)\sin\omega_1 + (N_2 + U_2 - T_2 \sin\omega_2)\sin\omega_2 - T_1 \cos\omega_1 \cos\omega_1 - T_2 \cos\omega_2 \cos\omega_2$$

$$= (N_1 + U_1)\sin\omega_1 + (N_2 + U_2)\sin\omega_2 - T_1 \sin^2\omega_1 - T_1 \cos^2\omega_1 - T_2 \sin^2\omega_2 - T_2 \cos^2\omega_2$$

$$= (N_1 + U_1)\sin\omega_1 + (N_2 + U_2)\sin\omega_2 - T_1 - T_2 \quad (5.1)$$

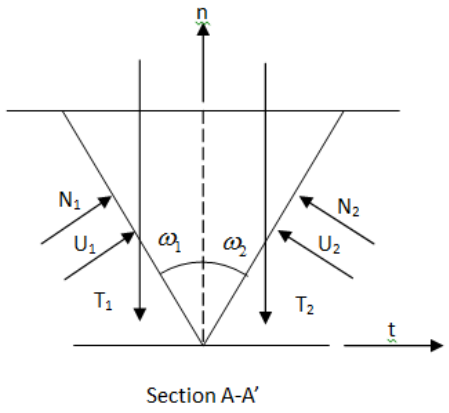

Fig. 5.1. Two-dimentional view of the section A-A' for system #1

5.2.2 Anchored system #2

As Fig.5.2 shows anchors perpendicular across the slope face through to the line of intersection for the stabilizing force T, assuming $T = T_1 + T_2$. The value of N is

$$N = (N_1 + U_1)\sin\omega_1 + (N_2 + U_2)\sin\omega_2 - T \quad (5.2)$$

If the equilibrium of forces in the directions of n and t is considered, the equations are

$$\sum F_n = W\left(\cos\psi_p - k_h \sin\psi_p \pm k_v \cos\psi_p\right) + Q\cos\psi_p - k_h Q\sin\psi_p \pm k_v Q\cos\psi_p + T\cos\alpha - N = 0 \quad (5.3)$$

and

$$\sum F_t = (N_1 + U_1)\cos\omega_1 - (N_2 + U_2)\cos\omega = 0 \quad (5.4)$$

where $N_1 + N_2$ is obtained from equations (5.2), (5.3) and (5.4):

$$N_1 + N_2 = \begin{bmatrix} W\left(\cos\psi_p - k_h \sin\psi_p \pm k_v \cos\psi_p\right) \\ + Q\cos\psi_p - k_h Q\sin\psi_p \pm k_v Q\cos\psi_p + T\cos\alpha + T \end{bmatrix} \lambda - U \quad (5.5)$$

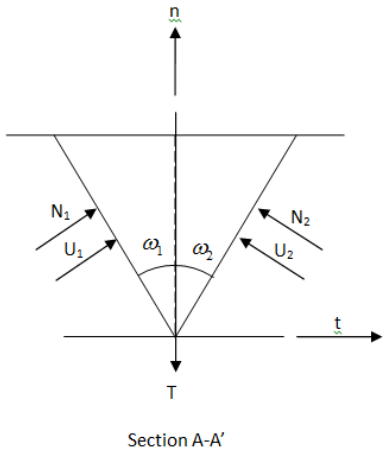

Fig. 5.2. Two-dimentional view of the section A-A' for system #2

5.2.3 Anchored system #3

As Fig. 5.3 shows anchors going through the slope face perpendicular to plane A and plane B for the stabilizing force T_1 and T_2, respectively. The N is

$$N = (N_1 + U_1 - T_1)\sin\omega_1 + (N_2 + U_2 - T_2)\sin\omega_2 \tag{5.6}$$

If the equilibrium of forces in the directions of n and t is considered, the equations are

$$\begin{aligned}\sum F_n = {} & W\left(\cos\psi_p - k_h \sin\psi_p \pm k_v \cos\psi_p\right) + Q\cos\psi_p \\ & - k_h Q\sin\psi_p \pm k_v Q\cos\psi_p + T\cos\alpha - N = 0\end{aligned} \tag{5.7}$$

and

$$\sum F_t = (N_1 + U_1 - T_1)\cos\omega_1 - (N_2 + U_2 - T_2)\cos\omega = 0 \tag{5.8}$$

where

$$N_1 + N_2 = \begin{bmatrix} W\left(\cos\psi_p - k_h \sin\psi_p \pm k_v \cos\psi_p\right) \\ + Q\cos\psi_p - k_h Q\sin\psi_p \pm k_v Q\cos\psi_p + T\cos\alpha \end{bmatrix}\lambda - U + T \tag{5.9}$$

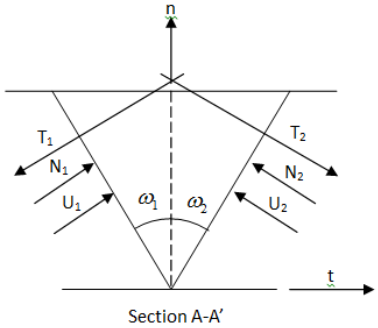

Fig. 5.3. Two-dimentional view of the section A-A' for system #3

As three systems shown, for comparing the system 1 and system 2, equation (5.1) and (5.2) would be compared as:

$$N = (N_1 + U_1)\sin\omega_1 + (N_2 + U_2)\sin\omega_2 - T_1 - T_2 \tag{5.1}$$

and

$$N = (N_1 + U_1)\sin\omega_1 + (N_2 + U_2)\sin\omega_2 - T \tag{5.2}$$

Those two equations are same if assuming $T = T_1 + T_2$. But for the case 2 is easy to show in two-dimensional vision, this case would be preferred.

The comparison of systems 2 and 3 is carried out by equationa (5.5) and (5.7) as:

$$\begin{aligned} N_1 + N_2 &= \begin{bmatrix} W\left(\cos\psi_p - k_h \sin\psi_p \pm k_v \cos\psi_p\right) \\ + Q\cos\psi_p - k_h Q\sin\psi_p \pm k_v Q\cos\psi_p + + T\cos\alpha + T \end{bmatrix}\lambda - U \\ &= \begin{bmatrix} W\left(\cos\psi_p - k_h \sin\psi_p \pm k_v \cos\psi_p\right) \\ + Q\cos\psi_p - k_h Q\sin\psi_p \pm k_v Q\cos\psi_p \end{bmatrix}\lambda - U + + T\lambda\cos\alpha + T\lambda \end{aligned} \tag{5.5}$$

and

$$\begin{aligned} N_1 + N_2 &= \begin{bmatrix} W\left(\cos\psi_p - k_h \sin\psi_p \pm k_v \cos\psi_p\right) \\ + Q\cos\psi_p - k_h Q\sin\psi_p \pm k_v Q\cos\psi_p + T\sin\omega\cos\alpha \end{bmatrix}\lambda - U + T \\ &= \begin{bmatrix} W\left(\cos\psi_p - k_h \sin\psi_p \pm k_v \cos\psi_p\right) \\ + Q\cos\psi_p - k_h Q\sin\psi_p \pm k_v Q\cos\psi_p \end{bmatrix}\lambda - U + T\lambda\sin\omega\cos\alpha + T \end{aligned} \tag{5.7}$$

The difference in the two equations is $T\lambda\cos\alpha + T\lambda$ and $T\lambda\sin\omega\cos\alpha + T$.

Comparing the 2 equations in two parts, firstly $T\lambda\cos\alpha$ and $T\lambda\sin\omega\cos\alpha$, $T\lambda\cos\alpha \geq T\lambda\sin\omega\cos\alpha$ because $\sin\omega$ always ≤ 1 and then comparing $T\lambda$ and T, the λ is the key point as:

$$\lambda = \frac{\cos\omega_1 + \cos\omega_2}{\sin(\omega_1 + \omega_2)} \tag{5.8}$$

In order to make equation simple, assume $\omega_1 = \omega_2$ or similar (the answer will not change much), thus:

$$\lambda = \frac{2\cos\omega_1}{\sin(2\omega_1)} = \frac{2\cos\omega_1}{2\sin\omega_1\cos\omega_1} = \frac{1}{\sin\omega_1} \text{ will always } \geq 1 \quad (5.9)$$

So $T\lambda$ always ≥ 1 T, system #2 is better than system #3.

According to the comparison, the system two is the best option to be carried out in the analytical formulation section.

5.3 General wedge failure conditions and assumptions

Figure 5.4(a) shows a three-dimensional view of a rock slope of height *H* with a tetrahedral wedge block bounded by intersecting joint planes POM (Plane 1) and OQM (Plane 2), which have OM as the line of intersection. The slope is inclined to the horizontal at ψ_f, and OM makes an angle of ψ_p with the horizontal. For convenience, the top face has been considered as rectangle $B \times L$. Figure 5.4(b) shows a two-dimensional view of the slope along a vertical section passing through line OM. Figure 5.1、5.2、5.3 showns three two-dimensional view of the slope alone a vertical section perpendicular to the line of intersection passing through line YY′ for three different cases, as named section Y-Y′. N_1 and N_2 is the nomal force acting on the plane 1 and plane 2, respectively. Plane 1 is inclinded to vertical at ω_1, and Plane 2 is inclined to vertical at ω_2. T is the stabilizing force, different case T acting different coordination. The weight of sliding block is W, and horizontal and verticle seismic forces, k_hW and k_vW, respectively (k_h and k_v are seismic coefficients) , are shown to act on the sliding block. A surcharge placed at the top of the slope applies a downward vertical pressure q. The horizontal and verticle seismic forces also considered on the surcharge, they are $k_hqBD/2$ and $k_vqBD/2$, respectively. The uplift forces due to water pressure on the joint plane 1 and plane 2 are U_1 and U_2, respectively. The anchoring stabilizing system is considered as force T inclined at an angle α to normal at the joint plane OM. N is the normal force acting perpendicular to the line of

intersection in a plane. *S* is the shear force. In order to have the sum of the forces acting on the line of intersection, the direction n is assumend perpendicular to the line of intersection.

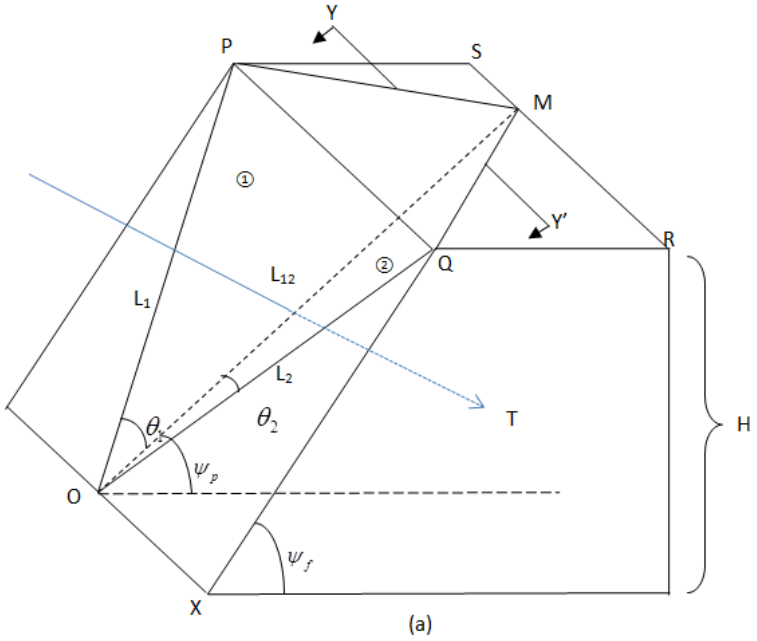

Fig. 5.4. (a) three-dimentional view of the rock slope

5.4 Analytical Derivation

The factor of safety (*FS*) of the rock slope is defined as a ratio of the resisting force F_r to the driving force F_i (Kovari and Fritz 1975; Hoek and Bray 1989). Thus

$$FS = \frac{F_r}{F_i} \tag{5.10}$$

It should be noted that F_r is the total force available to resist the block sliding on two wedge planes and F_i is the total force driving the rock wedge to sliding on the two planes.

The Mohr-Coulomb failure criterion (Lambe and Whitman, 1979; Das, 2008) is

$$F_r = cA + (N_1 + N_2)\tan\phi \tag{5.11}$$

where c is the cohesion, *A* is the total base area OPM and OQM, and N_1, N_2 are the normal forces acting on the failure plane 1 and plane 2, and ϕ is the angle of shearing

resistance of the material at the failure plane.

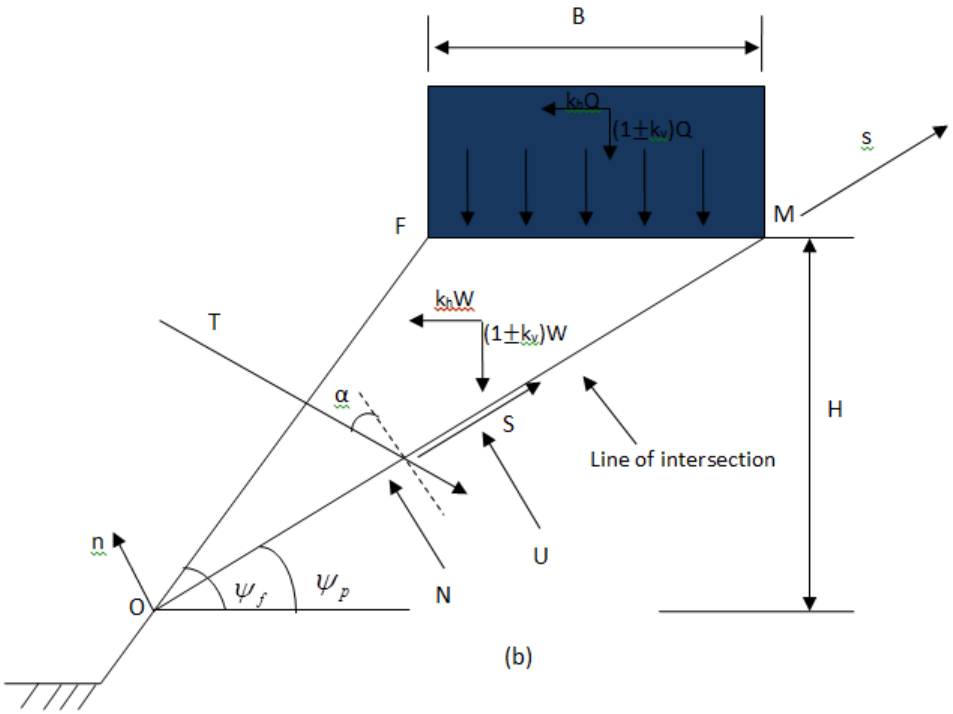

Fig. 5.4. (b) two-dimentional view of the rock slope

As Fig.5.4 (b) shows, sum of all the forces acting on the slope along the normal to the line of intersection is

$$\sum F_n = W\left(\cos\psi_p - k_h \sin\psi_p \pm k_v \cos\psi_p\right) + Q\cos\psi_p - k_h Q\sin\psi_p \pm k_v Q\cos\psi_p + T\cos\alpha - N = 0 \quad (5.12)$$

Sum of all the forces acting on the slope along the t direction as shown in Fig. 5.2, the equation is

$$\sum F_t = (N_1 + U_1)\cos\omega_1 - (N_2 + U_2)\cos\omega_2 = 0 \quad (5.13)$$

N is normal force acting on the line of intersection of the slope (Fig.5.2) as given below

$$N = (N_1 + U_1)\sin\omega_1 + (N_2 + U_2)\sin\omega_2 - T \quad (5.14)$$

Sum of normal forces on plane 1 and plane 2 can be obtained from simultaneous equations (5.12), (5.13) and (5.14) (the details are given in the appendix) as

$$N_1 + N_2 = \begin{bmatrix} W\left(\cos\psi_p - k_h \sin\psi_p \pm k_v \cos\psi_p\right) \\ + Q\cos\psi_p - k_h Q\sin\psi_p \pm k_v Q\cos\psi_p + T\cos\alpha + T \end{bmatrix}\lambda - U \tag{5.15}$$

Thus the total resisting forces is given as:

$$F_r = cA + \left\{\begin{bmatrix} W\left(\cos\psi_p - k_h \sin\psi_p \pm k_v \cos\psi_p\right) \\ + Q\cos\psi_p - k_h Q\sin\psi_p \pm k_v Q\cos\psi_p + T\cos\alpha + T \end{bmatrix}\lambda - U\right\}\tan\phi \tag{5.16}$$

The total driving force is calculated as:

$$\begin{aligned} F_i &= W\sin\psi_p + Wk_h\cos\psi_p \pm Wk_v\sin\psi_p \\ &\quad + Q\sin\psi_p + k_h Q\cos\psi_p \pm k_v Q\sin\psi_p - T\sin\alpha \\ &= (W+Q)\left[(1\pm k_v)\sin\psi_p + k_h\cos\psi_p\right] - T\sin\alpha \end{aligned} \tag{5.17}$$

From the equations (5.16) and (5.17), the factor of safety is

$$FS = \frac{F_r}{F_i} = \frac{cA + \left\{\begin{bmatrix} W\left(\cos\psi_p - k_h \sin\psi_p \pm k_v \cos\psi_p\right) \\ + Q\cos\psi_p - k_h Q\sin\psi_p \pm k_v Q\cos\psi_p + T\cos\alpha + T \end{bmatrix}\lambda - U\right\}\tan\phi}{(W+Q)\left[(1\pm k_v)\sin\psi_p + k_h\cos\psi_p\right] - T\sin\alpha} \tag{5.18}$$

The parameters A, W, σ_{sur}, λ and U are obtained as follows:

$$A = A_1 + A_2 = \frac{L_1 L_{12}\sin\theta_1}{2} + \frac{L_2 L_{12}\sin\theta_2}{2} = \frac{H(L_1\sin\theta_1 + L_2\sin\theta_2)}{2\sin\psi_p} \tag{5.19}$$

where A is the total connect area between failure plane and rock slope. θ_1 is the angle between L_1 and L_{12}, and θ_2 is the angle between L_2 and L_{12}.

The weight of the sliding rock mass block OREP is

$$W = \gamma V = \gamma H\frac{BD}{6} \tag{5.20}$$

where γ is the unit weight of rock mass.

The surcharge loading on the wedge block Q ($PQRS$ is a rectangular shape) is

$$Q = \frac{qBD}{2} \tag{5.21}$$

with

$$B = \frac{H}{\tan\psi_p} - \frac{H}{\tan\psi_f} = H(\cot\psi_p - \cot\psi_f) \tag{5.22}$$

where B represent *FM* in Fig. 5.4 (b).

λ is called the wedge factor by Kovari and Fritz (1975) as given below:

$$\lambda = \frac{\cos\omega_1 + \cos\omega_2}{\sin(\omega_1 + \omega_2)} \tag{5.23}$$

where ω_1, ω_2 are the angles between the surface A and the vertical and the angle between the surface B and the vertical, respectively.

Uplift force on the sliding block due to water pressure on failure planes 1 and 2 is

$$U = U_1 + U_2 = \frac{\gamma_w H}{6} A_u + \frac{\gamma_w H}{6} A_u = \frac{\gamma_w H}{3} A_u \tag{5.24}$$

where γ_w is the unit weight of water.

The cross-sectional area (*OJM*) of wedge block is

$$A_u = \frac{BH}{2} \tag{5.25}$$

Thus the equation of FS becomes

$$FS = \frac{F_r}{F_i}$$

$$= \frac{c\dfrac{H(L_1\sin\theta_1 + L_2\sin\theta_2)}{2\sin\psi_p} + \left\{\begin{bmatrix}\gamma H\dfrac{BD}{6}\left(\cos\psi_p - k_h\sin\psi_p \pm k_v\cos\psi_p\right) + \dfrac{qBD}{2}\cos\psi_p \\ -k_h\dfrac{qBD}{2}\sin\psi_p \pm k_v\dfrac{qBD}{2}\cos\psi_p + T\cos\alpha + T\end{bmatrix}\dfrac{\cos\omega_1 + \cos\omega_2}{\sin(\omega_1+\omega_2)} - \dfrac{\gamma_w BH^2}{6}\right\}\tan\phi}{\left(\gamma H\dfrac{BD}{6} + \dfrac{qBD}{2}\right)\left[(1\pm k_v)\sin\psi_p + k_h\cos\psi_p\right] - T\sin\alpha} \tag{5.26}$$

$$FS = \frac{F_r}{F_i}$$

$$= \frac{c\dfrac{H(L_1\sin\theta_1 + L_2\sin\theta_2)}{2\sin\psi_p} + \left\{\begin{bmatrix}\dfrac{BD}{6}\left(\cos\psi_p - k_h\sin\psi_p \pm k_v\cos\psi_p\right) \\ (\gamma H + 3q) + T(\cos\alpha + 1)\end{bmatrix}\dfrac{\cos\omega_1 + \cos\omega_2}{\sin(\omega_1+\omega_2)} - \dfrac{\gamma_w BH^2}{6}\right\}\tan\phi}{\frac{1}{6}BD(\gamma H + 3q)\left[(1\pm k_v)\sin\psi_p + k_h\cos\psi_p\right] - T\sin\alpha} \tag{5.27}$$

Dividing by γH^3, the equation becomes:

$$FS = \frac{F_r}{F_i}$$

$$= \frac{\dfrac{c(\frac{L_1}{H}\sin\theta_1 + \frac{L_2}{H}\sin\theta_2)}{2\gamma H \sin\psi_p} + \left\{ \begin{bmatrix} \frac{1}{6}\frac{D}{H}(\cot\psi_p - \cot\psi_f)\left(\cos\psi_p - k_h\sin\psi_p \pm k_v\cos\psi_p\right) \\ (1+3\frac{q}{\gamma H}) + \frac{T(\cos\alpha+1)}{\gamma H^3} \end{bmatrix} \frac{\cos\omega_1 + \cos\omega_2}{\sin(\omega_1+\omega_2)} \right\} \tan\phi}{\frac{1}{6}\frac{D}{H}(\cot\psi_p - \cot\psi_f)\left(1+\frac{3q}{\gamma H}\right)\left[(1\pm k_v)\sin\psi_p + k_h\cos\psi_p\right] - \frac{T\sin\alpha}{\gamma H^3}} \quad (5.28)$$

In order to find an easy way to work on the parametric analysis, the following nondimensional parameters are defined:

$$c^* = \frac{c}{\gamma H}, \gamma^* = \frac{\gamma}{\gamma_w}, q^* = \frac{q}{\gamma H}, L_1^* = \frac{L_1}{H}, L_2^* = \frac{L_2}{H}, D^* = \frac{D}{H}, T^* = \frac{T}{\gamma H^3}.$$

$$FS = \frac{F_r}{F_i}$$

$$= \frac{\dfrac{c^*(L_1^*\sin\theta_1 + L_2^*\sin\theta_2)}{2\sin\psi_p} + \left\{ \begin{bmatrix} [\frac{1}{6}D^*(\cot\psi_p - \cot\psi_f)\left(\cos\psi_p - k_h\sin\psi_p \pm k_v\cos\psi_p\right) \\ (1+3q^*)] + T*(\cos\alpha+1) \end{bmatrix} \frac{\cos\omega_1 + \cos\omega_2}{\sin(\omega_1+\omega_2)} \right\} \tan\phi}{\frac{1}{6}D^*(\cot\psi_p - \cot\psi_f)\left(1+3q^*\right)\left[(1\pm k_v)\sin\psi_p + k_h\cos\psi_p\right] - T^*\sin\alpha} \quad (5.29)$$

5.5 Special Cases

Case 1: The joint material is cohesionless, and there are no surcharge, seismic forces and water force, that is, $c^* = 0,\ \phi \neq 0, q^* = 0, T^* = 0, k_h = 0, k_v = 0,$ and $U = \dfrac{(\cot\psi_p - \cot\psi_f)}{6\gamma^*} = 0$.

The equation (5.29) becomes

$$FS = \frac{\lambda \tan\phi}{\tan\psi_p} \quad (5.30)$$

Case 2: The joint material is cohesionless, and there is no seismic forces and water in the tension crack, that is, $c^* = 0, \phi \neq 0, q^* = 0, T^* \neq 0, k_h = 0, k_v = 0$ and $U = 0$.

The equation (5.29) becomes

$$FS = \frac{F_r}{F_i} = \frac{\left\{\left[\left[\frac{1}{6}D^* \cos\psi_p(\cot\psi_p - \cot\psi_f)\right] + T^*(\cos\alpha + 1)\right]\frac{\cos\omega_1 + \cos\omega_2}{\sin(\omega_1 + \omega_2)}\right\}\tan\phi}{\frac{1}{6}D^* \sin\psi_p(\cot\psi_p - \cot\psi_f) - T^* \sin\alpha} \quad (5.31)$$

Case 3: The joint material is cohesive and there are no seismic forces and water in the tension crack, that is, $c^* = 0, \phi \neq 0, q^* \neq 0, T^* \neq 0, k_h = 0, k_v = 0$ and $U = 0$.

The equation (5.29) becomes

$$FS = \frac{F_r}{F_i} = \frac{\left\{\left[\left[\frac{1}{6}D^* \cos\psi_p(\cot\psi_p - \cot\psi_f)(1 + 3q^*)\right] + T^*(\cos\alpha + 1)\right]\frac{\cos\omega_1 + \cos\omega_2}{\sin(\omega_1 + \omega_2)}\right\}\tan\phi}{\frac{1}{6}D^* \sin\psi_p(\cot\psi_p - \cot\psi_f)(1 + 3q^*) - T^* \sin\alpha} \quad (5.32)$$

Case 4: The joint material is c - ϕ material, and there are no seismic forces and water in the tension crack, $c^* \neq 0, \phi = 0, q^* \neq 0, T^* \neq 0, k_h = 0, k_v = 0$ and $U = 0$.

The equation (5.29) becomes

$$FS = \frac{F_r}{F_i} = \frac{\frac{c^*(L_1^* \sin\theta_1 + L_2^* \sin\theta_2)}{2\sin\psi_p}}{\frac{1}{6}D^* \sin\psi_p(\cot\psi_p - \cot\psi_f)(1 + 3q^*) - T^* \sin\alpha} \quad (5.33)$$

Case 5: The joint material is c - ϕ material, and there are no seismic forces, that is, $c^* \neq 0, \phi \neq 0, q^* \neq 0, T^* \neq 0, k_h = 0, k_v = 0$ and $U = 0$.

The equation (5.29) becomes

$$FS = \frac{F_r}{F_i}$$

$$= \frac{\dfrac{c^*(L_1^* \sin\theta_1 + L_2^* \sin\theta_2)}{2\sin\psi_p} + \left\{ \begin{bmatrix} [\dfrac{1}{6} D^* \cos\psi_p (\cot\psi_p - \cot\psi_f) \\ (1+3q*)] + T^*(\cos\alpha + 1) \end{bmatrix} \dfrac{\cos\omega_1 + \cos\omega_2}{\sin(\omega_1 + \omega_2)} \right\} \tan\phi}{\dfrac{1}{6} D^* \sin\psi_p (\cot\psi_p - \cot\psi_f)(1+3q^*) - T^* \sin\alpha} \qquad (5.34)$$

Case 6: The joint material is c - ϕ material, and there are only horizontal seismic forces, that is, $c^* \neq 0, \phi \neq 0, q^* \neq 0, T^* \neq 0, k_h = 0, k_v = 0$ and $U \neq 0$.

The equation (5.29) becomes

$$FS = \frac{F_r}{F_i}$$

$$= \frac{\dfrac{c^*(L_1^* \sin\theta_1 + L_2^* \sin\theta_2)}{2\sin\psi_p} + \left\{ \begin{bmatrix} [\dfrac{1}{6} D^* \cos\psi_p (\cot\psi_p - \cot\psi_f) \\ (1+3q^*)] + T^*(\cos\alpha + 1) \\ -\dfrac{(\cot\psi_p - \cot\psi_f)}{6\gamma^*} \end{bmatrix} \dfrac{\cos\omega_1 + \cos\omega_2}{\sin(\omega_1 + \omega_2)} \right\} \tan\phi}{\dfrac{1}{6} D^* \sin\psi_p (\cot\psi_p - \cot\psi_f)(1+3q^*) - T^* \sin\alpha} \qquad (5.35)$$

Case 7: The joint material is c - ϕ material, and there are only horizontal seismic forces, that is, $c^* \neq 0, \phi \neq 0, q^* \neq 0, T^* \neq 0, k_h \neq 0, k_v = 0$ and $U \neq 0$.

The equation (5.29) becomes

$$FS = \frac{F_r}{F_i}$$

$$= \frac{\dfrac{c^*(L_1^* \sin\theta_1 + L_2^* \sin\theta_2)}{2\sin\psi_p} + \left\{ \begin{bmatrix} [\dfrac{1}{6} D^* (\cot\psi_p - \cot\psi_f)(\cos\psi_p - k_h \sin\psi_p) \\ (1+3q^*)] + T^*(\cos\alpha + 1) \\ -\dfrac{(\cot\psi_p - \cot\psi_f)}{6\gamma*} \end{bmatrix} \dfrac{\cos\omega_1 + \cos\omega_2}{\sin(\omega_1 + \omega_2)} \right\} \tan\phi}{\dfrac{1}{6} D^* (\cot\psi_p - \cot\psi_f)(1+3q^*)(\sin\psi_p + k_h \cos\psi_p) - T^* \sin\alpha} \qquad (5.36)$$

5.6 Variation of factor of safety for different special cases

Figure 5.2 shows the variation of factor of safety of the rock slope with angle of shearing resistance of the joint material for several possible field situations as above case 1 to case 7, considering a particular set of governing parameters in their non-dimensional form as: $\psi_f = 50°$, $\psi_p = 35°$, $c^* = 0.08$, $D^* = 0.6$, $\gamma^* = 2.5$, $L_1^* = L_2^* = 1.4$, $k_h = 0.1$, $k_v = 0.05$, $q^* = 0.25$, $T^* = 0.01$, $\theta_1 = \theta_2 = 25°$, $\alpha = 10°$ and $\omega_1 = \omega_2 = 30^\circ$. It is noted that the factor of safety of rock slope increases with an increase in ϕ, the rate of increase of factor of safety is higher for the greater value of ϕ. As expected, the cohesion and stabilizing force increase the factor of safety for any ϕ. From equations (5.35) and (5.36), it can be seen, the horizontal seismic force affects the factor of safety slightly with an increase in ϕ; the rightward seismic force make factor of safety of this slope higher for any ϕ. For the vertical seismic force, the upward direction of seismic force decrease the factor of safety for any ϕ. The water force and surcharge are both destabilizing forces for rock slope. Hence, they are decreasing the factor of safety of rock slope.

Figure 5.3 shows the variation of factor of safety of the rock slope with cohesion of the joint material for several possible field situations for the case 1 to 7, considering a particular set of governing parameters in their nondimensional form as $\psi_f = 50°$, $\psi_p = 35°$, $D^* = 0.6$, $\gamma^* = 2.5$, $L_1^* = L_2^* = 1.4$, $k_h = 0.1$, $k_v = 0.05$, $q^* = 0.25$, $T^* = 0.01$, $\theta_1 = \theta_2 = 25°$, $\alpha = 10°$ and $\omega_1 = \omega_2 = 30^\circ$. It is observed that the factor of safety increases almost linearly with an increase in cohesion. It also notes that the factor of safety reaches highest value when water force and seismic force equal to zero. The factor of safety becomes the lowest value when ϕ equal to zero.

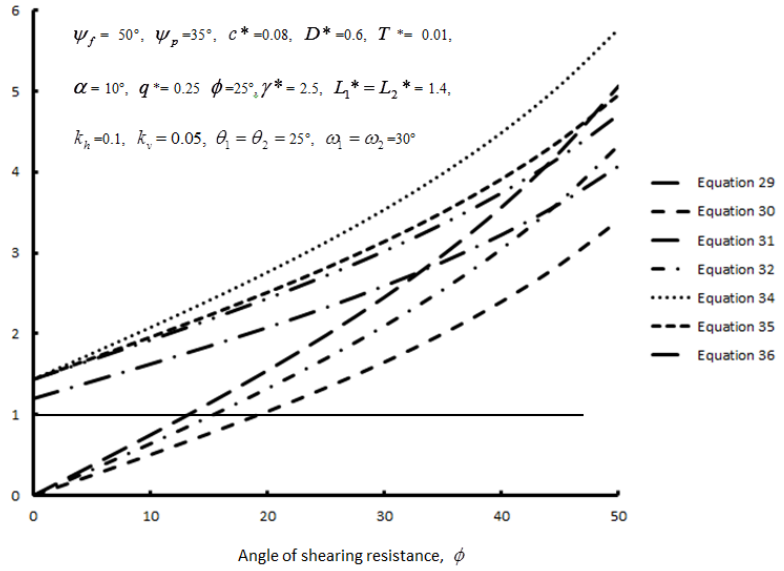

Fig. 5.5. Variation of factor of safety of the rock slope with angle of shearing resistance of the joint material for several possible field situations

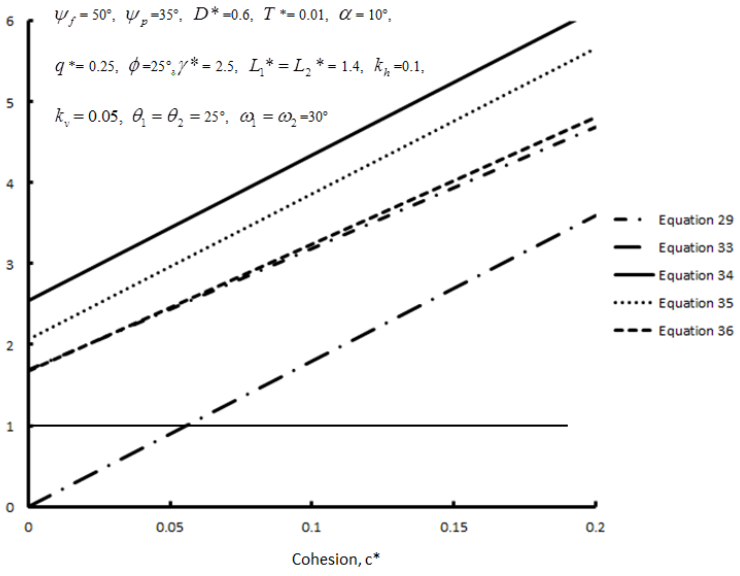

Fig. 5.6. Variation of factor of safety of the rock slope with cohesion of the joint material for several possible field situations

5.7 Conclusions

In this chapter, the nondimensional expression for the factor of safety against the wedge failure under surcharge and seismic force with anchors is derived as equation (5.20), with most forces which occur in the real field. Seven special cases are presented for several

possible field situations. It is observed that the factor of safety of the rock slope increases with an increase in both angle of shearing resistance and cohesion of the joint material. The value of factor of safety of equation (5.24) is always greater than others, because the water force and surcharge both are destabilizing forces for the rock slope. The horizontal seismic force decreases the factor of safety, whereas the vertical seismic force slightly affects the factor of safety.

Chapter 6

Parametric Study for Wedge Failure Analysis of Anchored Rock Slope

6.1 General

In this chapter, the parametric study is carried out for investigating the effects of governing parameters on the factor of safety which has been discussed in detail in Chapter 5. Effect of stabilizing force on the factor of safety with different values of governing parameters is also considered. There can be several slope geometries, and also a wide variation in joint and rock properties may take place in real field situations. For illustrative purpose, the parameters are assumed to be in the engineers' practical data range as presented in the following section.

6.2 Range of parameters

The parametric study has been made to investigate the effects of surcharge on the stability of rock slope. The considered ranges of parameters are shown below:

Angle of inclination of the failure plane to the horizontal	ψ_p : $30° - 45°$
Angle of inclination of the slope face to the horizontal	ψ_f : $40° - 60°$
Cohesion	c^*: 0 – 0.16
Angle of shearing resistance	ϕ: 20 – 40
Unit weight of rock	γ^*: 2.0– 2.8
Surcharge pressure	q^*: 0 – 1.6
Horizontal seismic coefficient	k_h : 0 – 0.4

Vertical seismic coefficient k_v : -0.15 – 0.15

Dips of planes 1 and 2 ω_1, ω_2 : $20^\circ - 30^\circ$

Stabilizing force T^* : 0 – 0.16

6.2.1 Effect of stabilizing force

Fig. 6.1 shows the variation of factor of safety (FS) with stabilizing force (T^*) for different values of cohesion (c^*) of the joint material along the sliding surface (c^*) as c^* = 0.00, 0.04, 0.08, 0.12 and 0.16; considering specific value of governing parameters in their nondimensional form as: ψ_f = 50°, ψ_p = 35°, γ^* = 2.5, , D^* = 0.6, ϕ = 25°, q^*=0.5, $L_1^* = L_2^* = 1.4$, k_h = 0.1, k_v = 0.05, α = 10°, $\theta_1 = \theta_2$ = 25° and $\omega_1 = \omega_2 = 30^\circ$. It is noticed that the factor of safety increases nonlinearly with an increase in stabilizing force when $c^* \neq 0$. The rate of increase is almost the same with an increase in stabilizing force for different values of cohesion with $c^* \neq 0$. When $c^* = 0$, the FS increases linearly with an increase in T^*. The greater value of the FS occurs with greater value of cohesion.

Fig. 6.2 shows the variation of factor of safety (FS) with stabilizing force (T^*) for different values of inclination of the slope face to the horizontal (ψ_f) as ψ_f = 40°, 45°, 50°, 55° and 60°; considering specific value of governing parameters in their nondimensional form as: ψ_p = 35°, γ^* = 2.5, c^* = 0.08, D^* = 0.6, ϕ = 25°, q^*=0.5, $L_1^* = L_2^* = 1.4$, k_h = 0.1, k_v = 0.05, α = 10°, $\theta_1 = \theta_2$ = 25° and $\omega_1 = \omega_2 = 30^\circ$. It is noticed that the factor of safety increases with an increase in the stabilizing force. The greater value of ψ_f makes the factor of safety smaller. The FS increases significantly when the ψ_f = 40°. When ψ_f = 50°, 55° and 60° , the FS increases almost linearly with an increase in the stabilizing force.

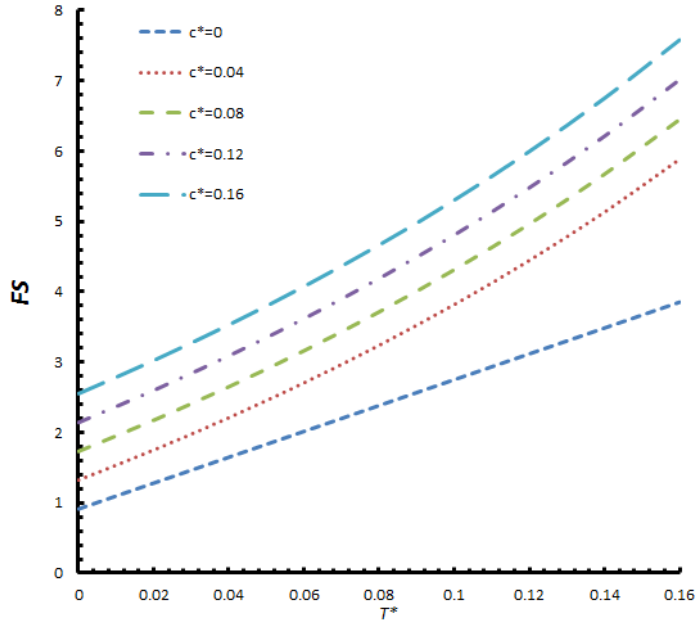

Fig. 6.1. Variation of factor of safety (FS) with stabilizing force (T^*) for different values of cohesion of the joint material along the sliding surface (c^*).

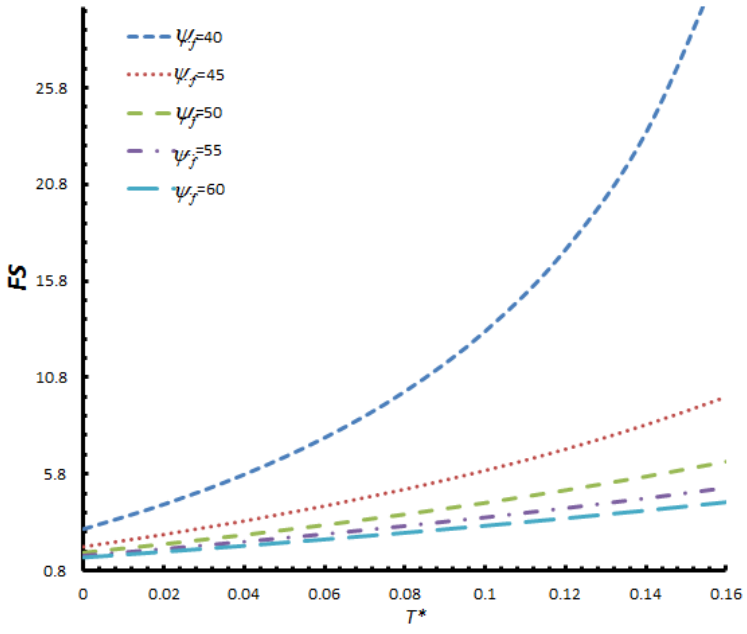

Fig. 6.2. Variation of factor of safety (FS) with stabilizing force (T^*) for different values of inclination of the slope face to the horizontal (ψ_f).

Fig. 6.3 shows the variation of the factor of safety (FS) with the stabilizing force (T^*) for different values of angle of inclination of failure plane to the horizontal (ψ_p) as ψ_p = 30°, 33°, 35°, 37° and 40°; considering specific value of governing parameters in their nondimensional form as: ψ_f = 50°, γ^* = 2.5, c^* = 0.08, D^* = 0.6, ϕ = 25°, q^* =0.5, $L_1^* = L_2^* = 1.4$, k_h = 0.1, k_v = 0.05, α = 10°, $\theta_1 = \theta_2$ = 25° and $\omega_1 = \omega_2 = 30^\circ$. It is observed that the factor of safety increases sharply with an increase in the stabilizing force. The FS also increases with an increase in the inclination of failure plane to the horizontal (ψ_p). The increase rate is the highest when ψ_p = 40°. It is also noted that the value of ψ_p between 30° and 40°, does not affect the FS much without stabilizing force.

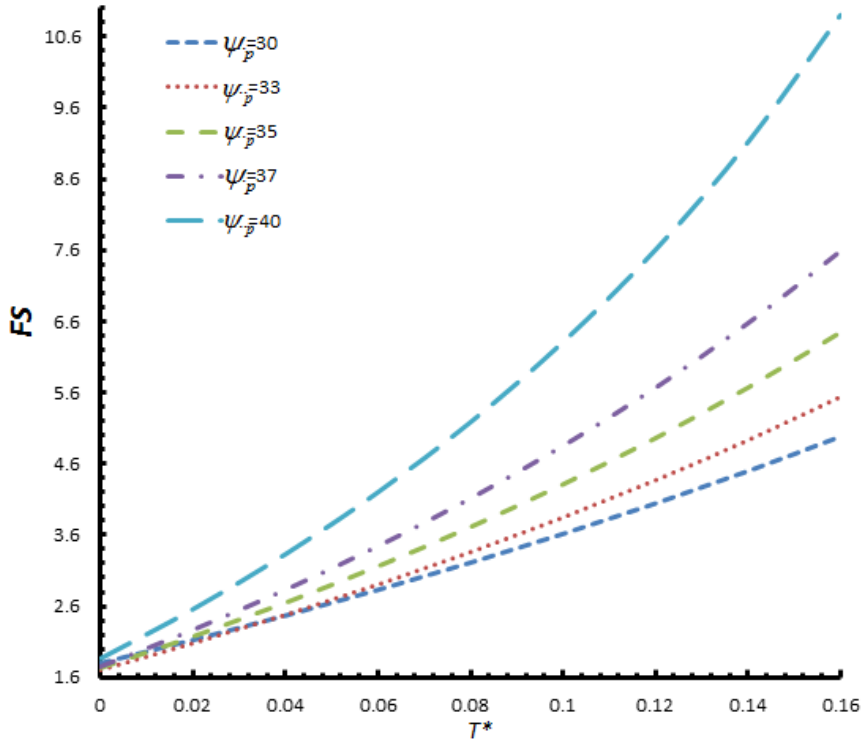

Fig. 6.3. Variation of factor of safety (FS) with stabilizing force (T^*) for different values of angle of inclination of failure plane to the horizontal (ψ_p).

Fig. 6.4 shows the variation of factor of safety (FS) with stabilizing force (T^*) for different values of horizontal seismic coefficient (k_h) as k_h = 0, 0.05, 0.1, 0.15, 0.2, 0.25 and 0.3; considering specific value of governing parameters in their nondimensional form as: ψ_f = 50°, ψ_p = 35°, γ^* = 2.5, c^* = 0.08, D^* = 0.6, ϕ = 25°, q^* =0.5, $L_1^* = L_2^* = 1.4$, k_v = 0.05, α = 10°, $\theta_1 = \theta_2$ = 25° and $\omega_1 = \omega_2 = 30^\circ$. It is noticed that the factor of safety increases almost linearly with an increase in the stabilizing force. The increasing rates are very similar for all range of horizontal seismic coefficient as figure shows. The FS increases with a decrease in horizontal seismic force.

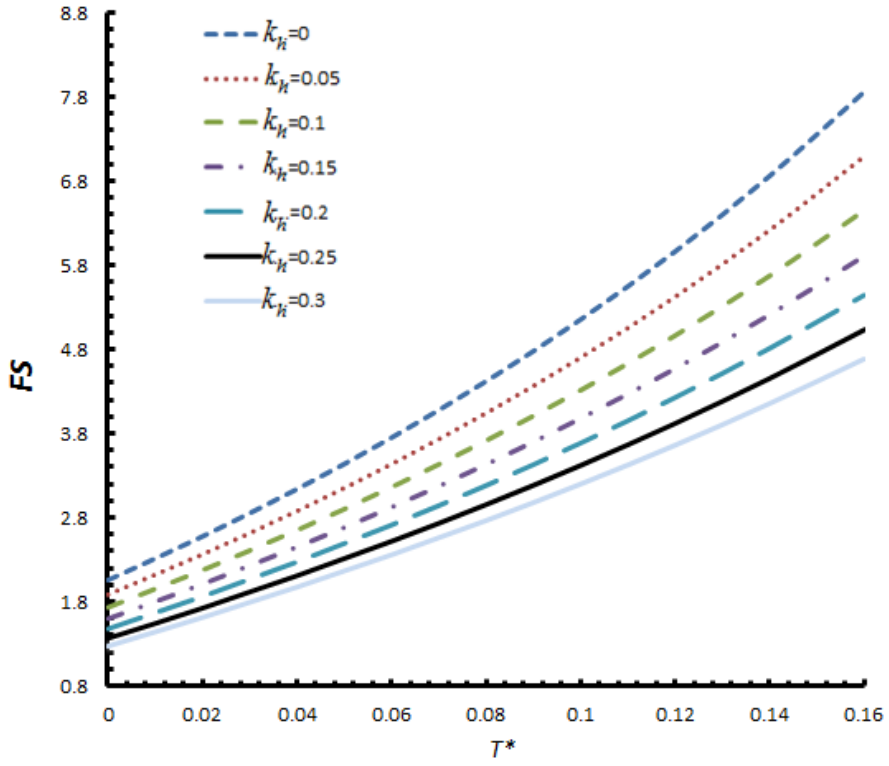

Fig. 6.4. Variation of factor of safety (FS) with stabilizing force (T^*) for different values of horizontal seismic coefficient (k_h).

Fig. 6.5 shows the variation of factor of safety (FS) with stabilizing force (T^*) for different values of vertical seismic coefficient (k_v) as k_v = -0.15, -0.1, -0.05, 0, 0.05, 0.1 and 0.15; considering specific value of governing parameters in their nondimensional form as: $\psi_f = 50°, \psi_p = 35°$, $\gamma^* = 2.5$, $c^* = 0.08$, $D^* = 0.6$, $\phi = 25°$, $q^* = 0.5$, $L_1^* = L_2^* = 1.4$, $k_h = 0.1$, $\alpha = 10°$, $\theta_1 = \theta_2 = 25°$ and $\omega_1 = \omega_2 = 30^\circ$. It is noted that the factor of safety increases significantly with an increase in the stabilizing force. The downward seismic force as positive value, it makes the FS decrease. The FS increases with a decrease in vertical seismic force. It is also noted that the k_v does not affect factor of safety much without stabilizing force.

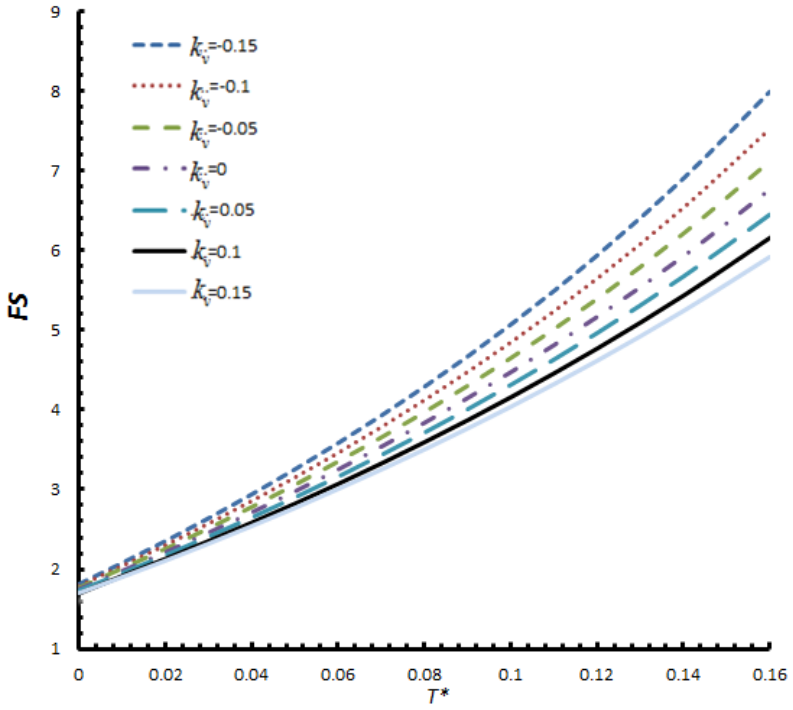

Fig. 6.5. Variation of factor of safety (FS) with stabilizing force (T^*) for different values of vertical seismic coefficient (k_v).

Fig. 6.6 shows the variation of factor of safety (FS) with stabilizing force (T^*) for different values of unit weight of rock (γ^*) as $\gamma^* = 2.5, 2.6, 2.7, 2.8$ and 2.9; considering

specific value of governing parameters in their nondimensional form as: ψ_f = 50°, ψ_p = 35°, c^* = 0.08, D^* = 0.6, ϕ = 25°, q^* =0.5, $L_1^* = L_2^* = 1.4$, k_h = 0.1, k_v = 0.05, α = 10°, $\theta_1 = \theta_2$ = 25° and $\omega_1 = \omega_2 = 30^\circ$. It is noticed that the factor of safety increase sharply with an increase in the stabilizing force. The FS increases very little with an increase in the unit weight of rock. The reason is that, the increase in the self-weight of rock gives rise to two components of the weight force. One acts on the sliding surface as a normal force, thus increasing the sliding resistance. The other one along the sliding direction acts as a driving force. Two forces go in an opposite direction, so they cancel each other such that the magnitude of γ^* has little effect.

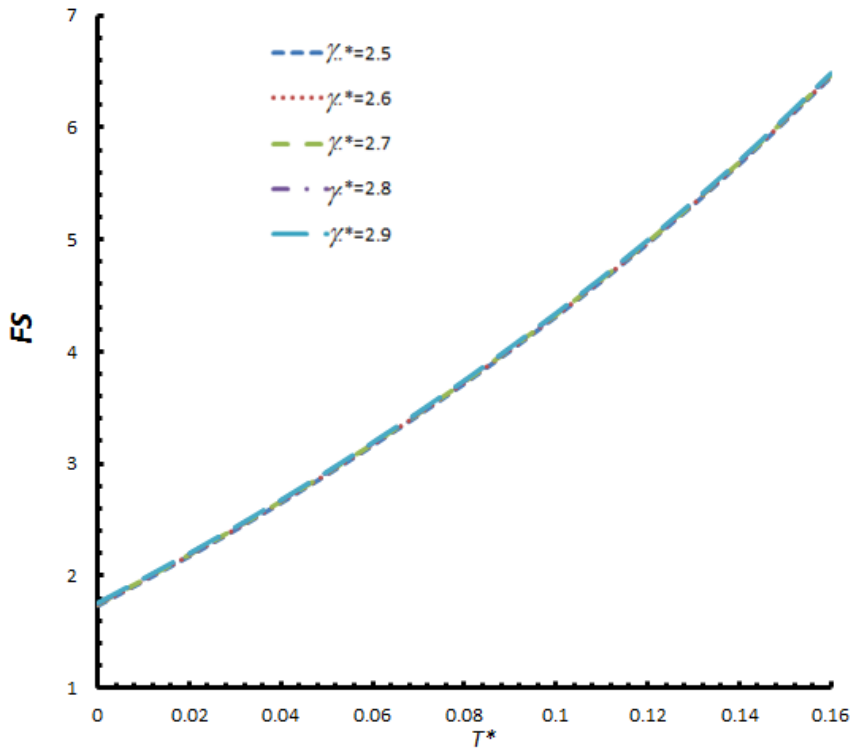

Fig. 6.6. Variation of factor of safety (FS) with stabilizing force (T^*) for different values of unit weight of rock (γ^*).

Fig. 6.7 shows the variation of factor of safety (FS) with stabilizing force (T^*) for different values of shearing resistance of the joint material along the sliding surface (ϕ) as ϕ =20°, 25°, 30°, 35° and 40°; considering specific value of governing parameters in their nondimensional form as: ψ_f = 50°, ψ_p = 35°, γ^* = 2.5, c^* = 0.08, D^* = 0.6, ϕ = 25°, q^* =0.5, $L_1^* = L_2^*$ = 1.4, k_h = 0.1, k_v = 0.05, α = 10°, $\theta_1 = \theta_2$ = 25° and $\omega_1 = \omega_2 = 30^\circ$. It is observed that the factor of safety increases with an increase in the stabilizing force. The FS also increases with an increase in the angle of shearing resistance of the joint material along the sliding surface.

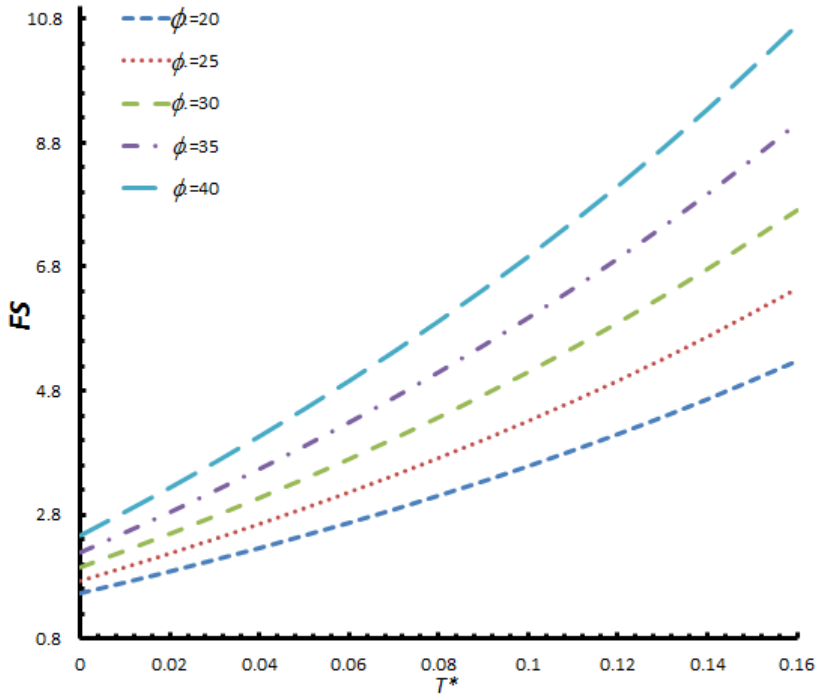

Fig. 6.7. Variation of factor of safety (FS) with stabilizing force (T^*) for different values of shearing resistance of the joint material along the sliding surface (ϕ).

6.2.2 Effect of angle of inclination of the slope face to the horizontal

Fig. 6.8 shows the variation of factor of safety (FS) with angle of inclination of the slope face to the horizontal (ψ_f) for different set values of horizontal (k_h) and vertical (k_v) seismic coefficients as 0.4, -0.2; 0.3, -0.15; 0.2, -0.1; 0.1, -0.05; 0, 0; 0.1, 0.05; 0.2, 0.1; 0.3, 0.15 and 0.4, 0.2; considering specific value of governing parameters in their nondimensional form as: ψ_p = 35°, γ^* = 2.5, c^* = 0.08, D^* = 0.6, ϕ = 25°, q^* =0.5, $L_1^* = L_2^* = 1.4$, T^* =0.05, α = 10°, $\theta_1 = \theta_2$ = 25° and $\omega_1 = \omega_2 = 30^\circ$. It is noticed that the factor of safety decreases sharply with an increase in the angle of inclination of the slope face to the horizontal. The decreasing rate is higher between range of 40° and 45°. When the horizontal and vertical seismic coefficients both equal to 0, the value of the FS is always bigger than other set of seismic coefficient. It proves that the seismic coefficients are the negative affect for the slope stability. In addition, the value of the FS is bigger with negative value of vertical seismic coefficient for the same value of horizontal seismic coefficient. It may be because the negative vertical seismic coefficient supplies an uplift force to resist rock block sliding.

6.2.3 Effect of angle of inclination of failure plane to the horizontal

Fig. 6.9 shows the variation of factor of safety (FS) with angle of inclination of failure plane to the horizontal (ψ_p) for different set values of horizontal (k_h) and vertical (k_v) seismic coefficients as 0.4, -0.2; 0.3, -0.15; 0.2, -0.1; 0.1, -0.05; 0, 0; 0.1, 0.05; 0.2, 0.1; 0.3, 0.15 and 0.4, 0.2; considering specific value of governing parameters in their nondimensional form as: ψ_f = 50°, γ^* = 2.5, c^* = 0.08, D^* = 0.6, ϕ = 25°, q^* =0.5, $L_1^* = L_2^* = 1.4$, T^* =0.05, α = 10°, $\theta_1 = \theta_2$ = 25° and $\omega_1 = \omega_2 = 30^\circ$. It is observed that the factor of safety increases moderately with an increase in stabilizing force between 30° and 42°, and it rises sharply after 42°. The value of the FS is the greatest when k_h = 0, k_v = 0. The lowest value of the FS occurs when k_h = 0.4, k_v = 0.2. From the figure as can be seen, the rock anchor is a good way to stabilize the unstable slope.

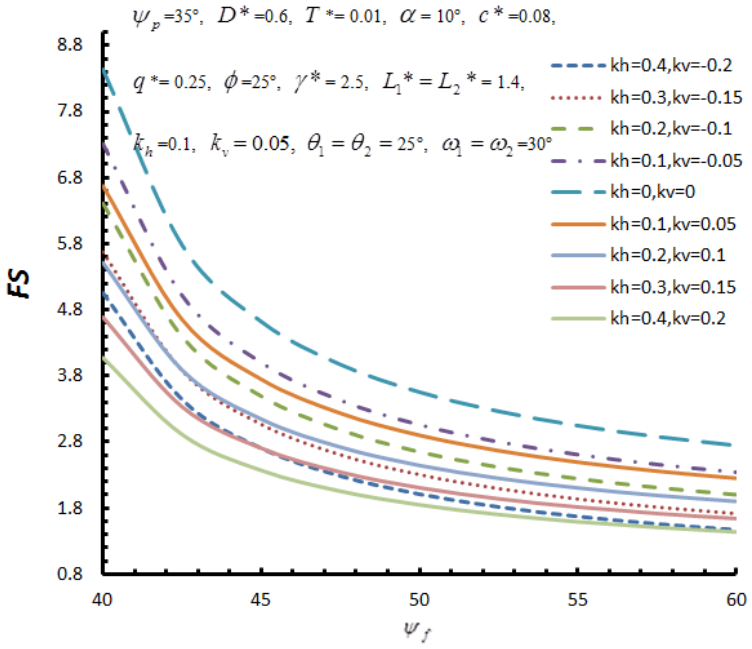

Fig. 6.8. Variation of factor of safety (FS) with angle of inclination of the slope face to the horizontal (ψ_f) for different set values of horizontal (k_h) and vertical (k_v) seismic coefficients.

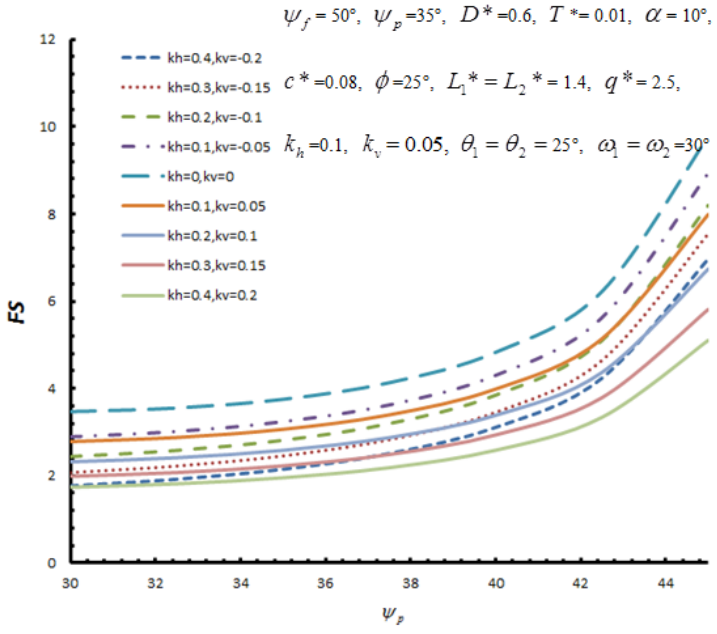

Fig. 6.9. Variation of factor of safety (FS) with angle of inclination of failure plane to the horizontal (ψ_p) for different values of horizontal (k_h) and vertical (k_v) seismic coefficients.

6.2.4 Effect of unit weight of rock

Fig. 6.10 shows the variation of factor of safety (FS) with different nondimensional values of unit weight of rock (γ^*) for different set values of horizontal (k_h) and vertical (k_v) seismic coefficients as 0.4, -0.2; 0.3, -0.15; 0.2, -0.1; 0.1, -0.05; 0, 0; 0.1, 0.05; 0.2, 0.1; 0.3, 0.15 and 0.4, 0.2; considering specific value of governing parameters in their nondimensional form as: $\psi_f = 50°$, $\psi_p = 35°$, $c^* = 0.08$, $D^* = 0.6$, $\phi = 25°$, $q^* = 0.5$, $L_1^* = L_2^* = 1.4$, $T^* = 0.05$, $\alpha = 10°$, $\theta_1 = \theta_2 = 25°$ and $\omega_1 = \omega_2 = 30^\circ$. It is noted that the factor of safety almost stays the same with an increase in unit weight of rock for any set of seismic coefficient. It may because the unit weight of rock affects the resisting force and driving force similarly.

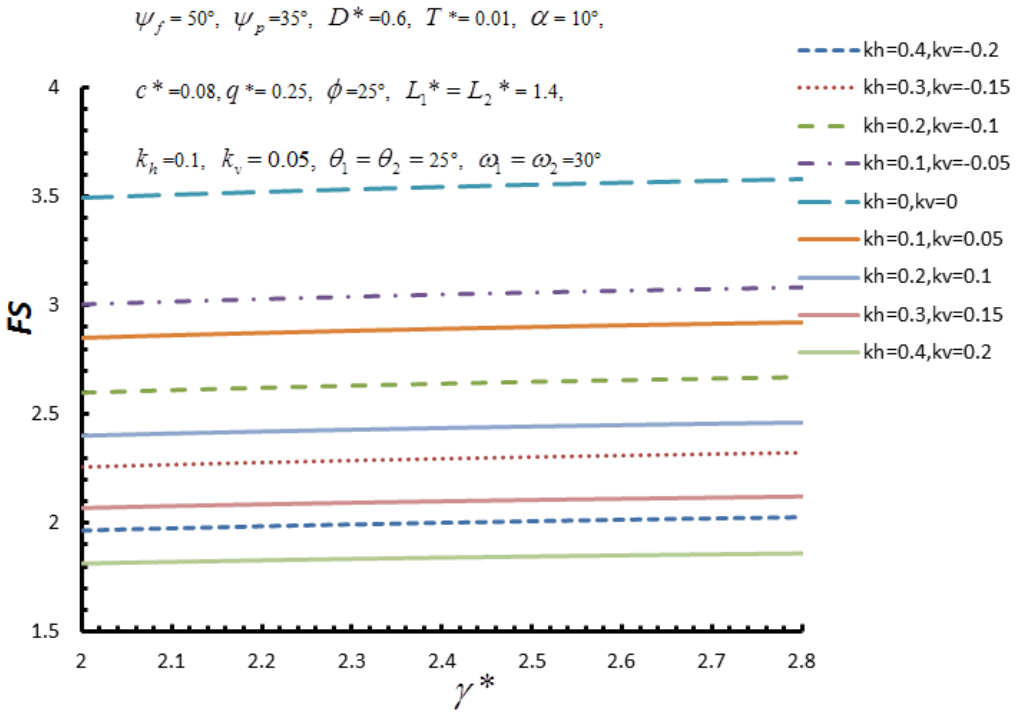

Fig. 6.10. Variation of factor of safety (FS) with different nondimensional values of unit weight of rock (γ^*) for different values of horizontal (k_h) and vertical (k_v) seismic coefficients.

6.2.5 Effect of surcharge

Fig. 6.11 shows the variation of factor of safety (FS) with nondimensional values of surcharge (q^*) for different values of horizontal (k_h) and vertical (k_v) seismic coefficients as 0.4, -0.2; 0.3, -0.15; 0.2, -0.1; 0.1, -0.05; 0, 0; 0.1, 0.05; 0.2, 0.1; 0.3, 0.15 and 0.4, 0.2; considering the specific value of governing parameters in their nondimensional form as: ψ_f = 50°, ψ_p = 35°, γ^* = 2.5, c^* = 0.08, D^* = 0.6, ϕ = 25°, $L_1^* = L_2^* = 1.4$, T^* =0.05, α = 10°, $\theta_1 = \theta_2$ = 25° and $\omega_1 = \omega_2 = 30^\circ$. It is observed that the factor of safety decreases nonlinearly with an increase in surcharge. It decreases sharply as surcharge increases from 0 to 0.5. The FS is reduced moderately as q^* increases after 0.5.

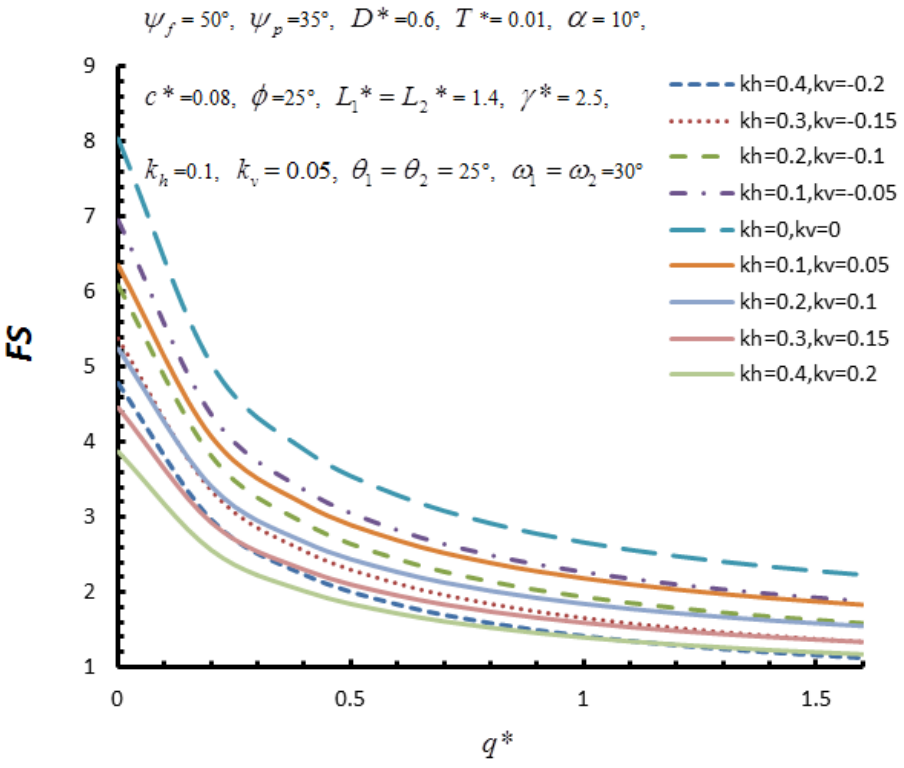

Fig. 6.11. Variation of factor of safety (FS) with nondimensional values of surcharge (q^*) for different values of horizontal (k_h) and vertical (k_v) seismic coefficients.

6.2.6 Effect of stabilizing force

Fig. 6.12 shows the variation of factor of safety (FS) with nondimensional values of stabilizing force (T^*) for different values of horizontal (k_h) and vertical (k_v) seismic coefficient as 0.4, -0.2; 0.3, -0.15; 0.2, -0.1; 0.1, -0.05; 0, 0; 0.1, 0.05; 0.2, 0.1; 0.3, 0.15 and 0.4, 0.2; considering the specific value of governing parameters in their nondimensional form as: $\psi_f = 50°$, $\psi_p = 35°$, $\gamma^* = 2.5$, $c^* = 0.08$, $D^* = 0.6$, $\phi = 25°$, $q^* = 0.5$, $L_1^* = L_2^* = 1.4$, $\alpha = 10°$, $\theta_1 = \theta_2 = 25°$ and $\omega_1 = \omega_2 = 30^\circ$. It is noted that the factor of safety increases moderately with an increase in stabilizing force. The value of the FS is the greatest when seismic forces are zero.

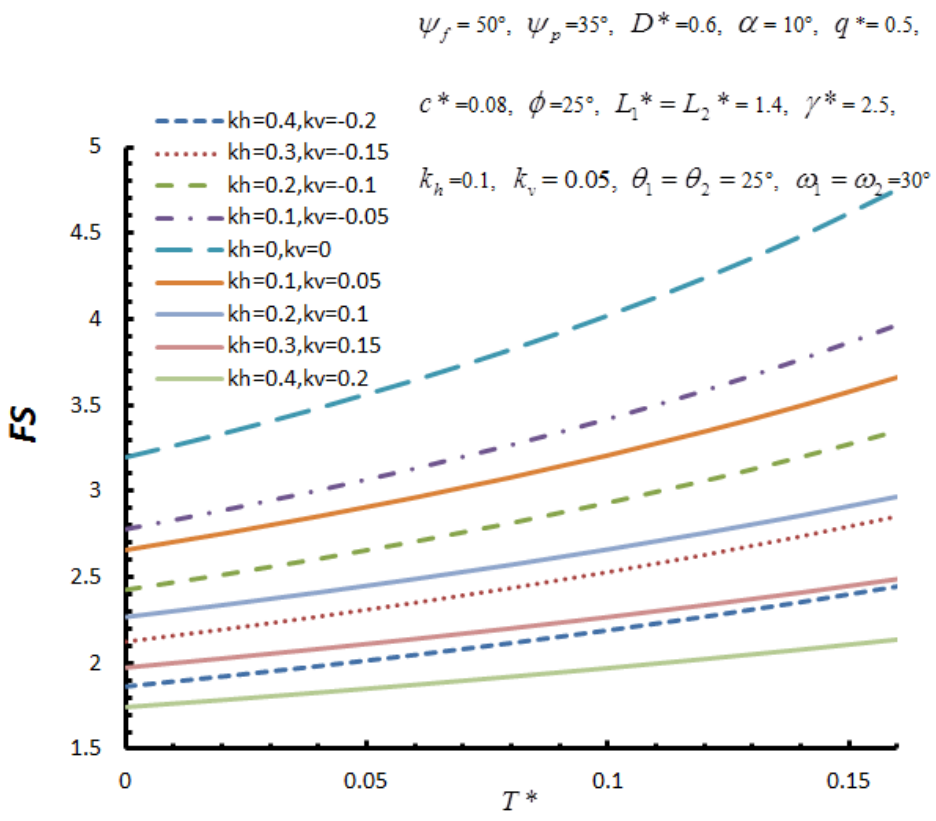

Fig. 6.12. Variation of factor of safety (FS) with different nondimensional values of stabilizing force (T^*) for different values of horizontal (k_h) and vertical (k_v) seismic coefficient.

6.2.7 Effect of inclination of stabilizing force to the normal at the failure plane

Fig. 6.13 shows the variation of factor of safety (FS) with inclination of stabilizing force to the normal at the failure plane (α) for different values of horizontal (k_h) and vertical (k_v) seismic coefficients as 0.4, -0.2; 0.3, -0.15; 0.2, -0.1; 0.1, -0.05; 0, 0; 0.1, 0.05; 0.2, 0.1; 0.3, 0.15 and 0.4, 0.2; considering the specific value of governing parameters in their nondimensional form as: $\psi_f = 50°$, $\psi_p = 35°$, $\gamma^* = 2.5$, $c^* = 0.08$, $D^* = 0.6$, $\phi = 25°$, $q^* = 0.5$, $L_1^* = L_2^* = 1.4$, $\theta_1 = \theta_2 = 25°$, $T^* = 0.05$, $\alpha = 10°$ and $\omega_1 = \omega_2 = 30^\circ$. It is observed that the factor of safety increases with an increase in inclination of stabilizing force to the normal at the failure plane. The FS arrives a peak value when the α increases to 80°.

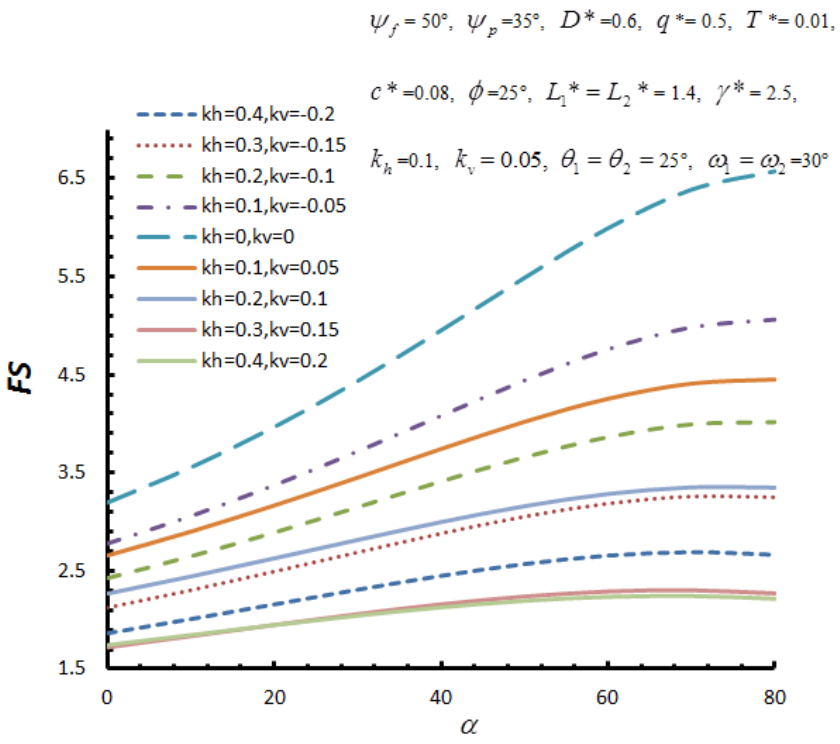

Fig. 6.13. Variation of factor of safety (FS) with inclination of stabilizing force to the normal at the failure plane (α) for different values of horizontal (k_h) and vertical (k_v) seismic coefficients.

6.2.8 Effect of cohesion of the joint material along the sliding surface

Fig. 6.14 shows the variation of factor of safety (FS) with cohesion of the joint material along the sliding surface (c^*) for different values of horizontal (k_h) and vertical (k_v) seismic coefficients as 0.4, -0.2; 0.3, -0.15; 0.2, -0.1; 0.1, -0.05; 0, 0; 0.1, 0.05; 0.2, 0.1; 0.3, 0.15 and 0.4, 0.2; considering the specific value of governing parameters in their nondimensional form as: $\psi_f = 50°$, $\psi_p = 35°$, $\gamma^* = 2.5$, $D^* = 0.6$, $\phi = 25°$, $q^* = 0.5$, $L_1^* = L_2^* = 1.4$, $\theta_1 = \theta_2 = 25°$, $T^* = 0.05$, $\alpha = 10°$ and $\omega_1 = \omega_2 = 30^\circ$. It is observed that the factor of safety increases linearly with an increase in cohesion. It may due to linear relationship of cohesion with shear strength as defined by the Mohr-Coulomb failure criterion. The greater value of the FS occurs with the lower value of seismic coefficients.

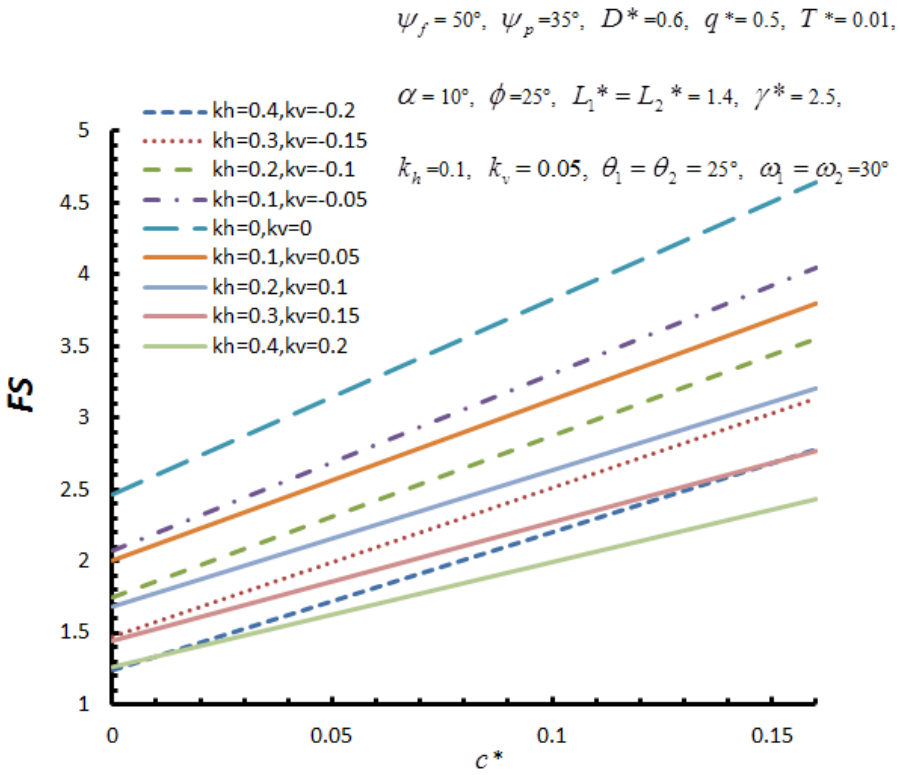

Fig. 6.14. Variation of factor of safety (FS) with cohesion of the joint material along the sliding surface (c^*) for different values of horizontal (k_h) and vertical (k_v) seismic coefficients.

6.2.9 Effect of angle of shearing resistance of the joint material along the sliding surface

Fig. 6.8 shows the variation of factor of safety (FS) with angle of shearing resistance of the joint material along the sliding surface (ϕ) for different values of horizontal (k_h) and vertical (k_v) seismic coefficients as 0.4, -0.2; 0.3, -0.15; 0.2, -0.1; 0.1, -0.05; 0, 0; 0.1, 0.05; 0.2, 0.1; 0.3, 0.15 and 0.4, 0.2; considering specific value of governing parameters in their nondimensional form as: $\psi_f = 50°$, $\psi_p = 35°$, $\gamma^* = 2.5$, $c^* = 0.08$, $D^* = 0.6$, $q^* = 0.5$, $L_1^* = L_2^* = 1.4$, $\theta_1 = \theta_2 = 25°$, $T^* = 0.05$, $\alpha = 10°$ and $\omega_1 = \omega_2 = 30^\circ$. It is noted that the factor of safety increases almost linearly with increase in angle of shearing resistance. It may due to linear relationship of the Mohr-Coulomb failure criterion.

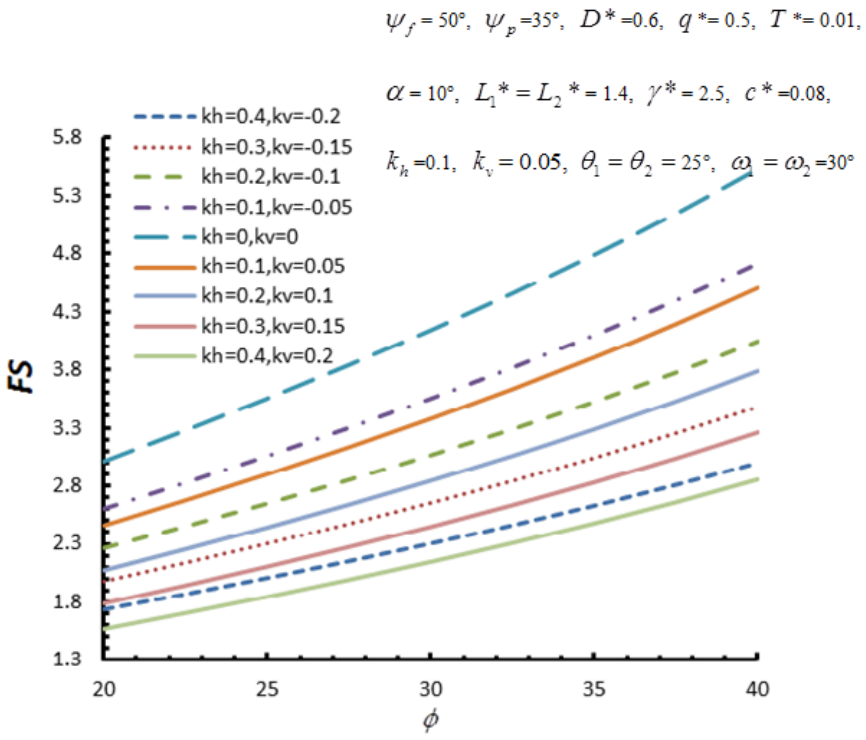

Fig. 6.15. Variation of factor of safety (FS) with angle of shearing resistance of the joint material along the sliding surface (ϕ) for different values of horizontal (k_h) and vertical (k_v) seismic coefficients.

6.3 Conclusions

The parametric study, presented in the previous sections, is used to investigate the effects of stabilizing force on the stability of rock slope. It also indicates that the effects of several other parameters on the factor of safety (FS) of rock slope. The factor of safety of rock slope increases with an increase in stabilizing force. The FS increases linearly with an increase in the stabilizing force when $c^* = 0$. The FS increases significantly with an increase in the stabilizing force when ψ_f = 40°, the rate of increase is much greater than that for values of angles other than between 40° to 60°. The FS increases with an increase in the angle of inclination of failure plane to the horizontal. The seismic loads as the destabilizing forces make the FS decrease. The FS decreases with an increase in seismic coefficient. However, the different unit weights of rock does not affect the FS significantly. The increase in the angle of shearing resistance triggers an increase in the FS.

Increasing ψ_f and q^* makes the FS decrease; whereas, the FS increases with an increase in T^*, ψ_p, α, c^* and ϕ. It is also found, the FS almost remains stable with an increase in γ^*.

Chapter 7

Summary and Conclusions

7.1 Summary

The stability of natural and man-made slopes is a very important task for civil and mining engineers, because the potential rock-falls result in a significant cost and serious personnel safety problem to the operators. In these situations, the slope stability assessment becomes crucial for the engineering work and for the economy. As the geological discontinuities exist in all rock types, the rock mass is generally governed by the geometrical distribution and mechanical properties of the discontinuities. The slope failure types have been classified by engineers in 5 types, such as plane failure, circular failure, wedge failure, toppling failure and buckling failure. Many researchers make a great effort in slope stability analysis, which has been well documented in the literature (Hoek and Bray 1981; Aydan *et al.* 2008; Aydan and Kumsar 2010; Nawari *et al.* 1997). Furthermore, the wedge failure of rock slope is probably the most common type of failure in rock sliding (Hoek and Bray, 1981). In order to analyse the stability of rock slope against the wedge failure, some of the methods have been applied for the wedge failure analysis, such as stereographic method, closed-form method, reliability method and limit equilibrium method (Hoek *et al.* 1973; Low and Einstein, 1992; Bjerager, 1990; Ling and Cheng, 1997).

The limit equilibrium approach for the estimation of the factor of safety of the rock slope against the wedge failure, is well accepted by the engineers, mainly because of simplicity in the development of explicit expressions and their frequent applications over a long period of time. Hoek and Bray (1981) presented the most basic limit equilibrium method to analyse the slope stability. FHWA (1989) reports that a factor of safety of 1.3 is adequate for low slopes and a factor of safety of 1.5 is required for critical slopes adjacent to major highways. Ling and Cheng (1997) extend the expression of factor of safety against the wedge failure under seismic coefficient. Kumsar *et al.* (2000) considered both water and seismic forces in the

wedge failure system. Basha *et al.* (2013) developed an expression for the factor of safety of rock slope against the wedge failure under water and seismic forces more clearly. As in the past studies, the anchor force and surcharge have not been mentioned; the expression of the factor of safety against the wedge failure under surcharge and seismic load has been derived in two systems, with anchors and without anchors in the present work. Several special cases of the factor of safety for different simplified field situations are presented in this thesis.

The graphical presentations for most of the practically occurring parameters within the typical ranges in the parametric study indicates the effects of governing parameters on the factor of safety. As the parametric study shows that the surcharge would always be a destabilizing force when the c^* is not zero, the factor of safety (FS) decreases with an increase in surcharge. However, when $c^* = 0$, the FS increases slightly with an increase in surcharge. The T^* would always be a stabilizing force that makes the FS to increase with an increase in T^*. The parametric study also shows how other governing parameters affect the factor of safety. As the ψ_p increases, the FS increases while it deceases with an increase in the ψ_f. It also observed that the FS decreases with an increase in k_h and k_v, separately, while it increases with an increases in the following parameters: α, c^* and ϕ. However, γ^* does not affect the FS significantly.

7.2 Conclusions

Based on the results of this study, the following conclusions are made:

- The expression for the factor of safety of a rock slope against the wedge failure under surcharge and seismic loads without anchors is given by equation (3.20), incorporating most of the practically occurring destabilizing forces.
- Six special cases of the equation (3.20) based on possible situations in the field have been presented.
- The factor of safety increases with an increase in both cohesion and the angle of shearing resistance for any possible field situation case. The value of the factor of safety of

equation (3.24) is always greater than others, because the water force and surcharge both are destabilizing forces for the rock slope. The horizontal seismic force decreases the factor of safety, whereas the vertical seismic force slightly affects the factor of safety.

- The factor of safety of rock slope decreases with an increase in surcharge. For the lower values of surcharge, the factor of safety decreases relatively faster.
- The factor of safety is relatively higher with greater value of cohesion and angle of shearing resistance with any surcharge. The factor of safety shows a rapid decreasing trend with an increase in surcharge for greater values of cohesion.
- The factor of safety decreases with almost the same trend with an increase in surcharge for any angle of shearing resistance.
- The factor of safety increases with an increase in unit weight of rock, but the factor of safety is not much affected by variation in unit weight of rock for any value of surcharge.
- The factor of safety increases with an increase in the values of angle of inclination of the slope face to the horizontal. While the FS increases with an increase in the values of angle of inclination of the failure plane to the horizontal (ψ_p) for lower values of surcharge (less than 1.5); it increases with a decrease in ψ_p for greater value of surcharge (greater than 1.5).
- The analytical expression of the factor of safety of rock slope against the wedge failure under surcharge and seismic load with anchors has been presented as equation (5.28). The seven special cases of equation (5.28) for possible field situations have been illustrated.
- The graphical analysis of seven special cases illustrated that the factor of safety of the rock slope increases with an increase in both angle of shearing resistance and cohesion of the joint material. The value of factor of safety of equation (5.24) is always greater than others, because the water force and surcharge both are destabilizing forces for the rock slope. For seismic force, the horizontal one decreases the factor of safety, whereas the vertical seismic force slightly affects the factor of safety.

- The parametric study of anchored rock slope against the wedge failure is graphically to investigate the effect of stabilizing force on the factor of safety. It is also indicated that the effects of other parameters for factor of safety of rock slope.
- The factor of safety increases linearly with an increase in the stabilizing force when $c^* = 0$. The factor of safety increases significantly with an increase in the stabilizing force when ψ_f = 40°, the increase rate is much greater than that for values of angles other than between 40° to 60°. The factor of safety increases with an increase in the angle of inclination of failure plane to the horizontal.
- The seismic forces as the destabilizing forces make the factor of safety decrease. It decreases as the seismic coefficient increases. However, the different unit weights of rock do not affect the factor of safety much. An increase in the angle of shearing resistance triggers an increase the factor of safety.
- Increasing ψ_f and q^* makes the factor of safety decrease; while the factor of safety increases with an increase in T^*, ψ_p, α, c^* and ϕ. In general, γ^* affect the factor of safety differently to others.
- The unit weight of rock γ^* does not affect the factor of safety significantly.

7.3 Recommendations for future work

The problems concerning the slope stability have been studied for several decades. The slope stability analysis is very important for many areas, such as road construction, dam installation and mine excavation. In this study, the factor of safety against the wedge failure under seismic and surcharge loads with anchors and without anchors have both been analysed. The parametric study is also presented to analyse the effect of several parameters on the factor of safety for both systems. The current research work can be extended further to consider the following:

- Development of a generalised expression for other failure modes including toppling failure or buckling failure under surcharge and seismic load conditions.

- Identify the analytical results by comparison with the results obtained from the numerical analysis.
- Analyse the wedge failure of anchored rock slope under surcharge and seismic load sconditions by reliability or stereographic analysis method.
- If possible, using the experimental results compare the value of factor of safety obtained from analytical study.
- Effects of other reinforcing techniques on the stability of rock slopes.
- Providing some design charts for real field projects, those that are more convenient for engineers.

Appendix

$$\sum F_n = W\left(\cos\psi_p - k_h \sin\psi_p \pm k_v \cos\psi_p\right) + Q\cos\psi_p - k_h Q\sin\psi_p \pm k_v Q\cos\psi_p - N = 0 \quad (1)$$

$$\sum F_t = (N_1 + U_1)\cos\omega_1 - (N_2 + U_2)\cos\omega_2 = 0 \quad (2)$$

$$N = (N_1 + U_1)\sin\omega_1 + (N_2 + U_2)\sin\omega_2 \quad (3)$$

From equation (2)

$$(N_1 + U_1)\cos\omega_1 = (N_2 + U_2)\cos\omega_2$$

$$N_1 + U_1 = \frac{(N_2 + U_2)\cos\omega_2}{\cos\omega_1} \quad (4)$$

Substitute the $N_1 + U_1$ to equation (3), as

$$N = \frac{(N_2 + U_2)\cos\omega_2}{\cos\omega_1}\sin\omega_1 + (N_2 + U_2)\sin\omega_2$$

$$= \frac{(N_2 + U_2)\cos\omega_2 \sin\omega_1}{\cos\omega_1} + \frac{(N_2 + U_2)\sin\omega_2 \cos\omega_1}{\cos\omega_1}$$

$$= \frac{(N_2 + U_2)\sin(\omega_1 + \omega_2)}{\cos\omega_1} \quad (5)$$

thus

$$N_2 + U_2 = \frac{N\cos\omega_1}{\sin(\omega_1 + \omega_2)} \quad (6)$$

From equation (2)

$$(N_1 + U_1)\cos\omega_1 = (N_2 + U_2)\cos\omega_2$$

$$N_2 + U_2 = \frac{(N_1 + U_1)\cos\omega_1}{\cos\omega_2} \quad (7)$$

Substitute the $N_2 + U_2$ to equation (3), as

$$N = (N_1 + U_1)\sin\omega_1 + \frac{(N_1 + U_1)\cos\omega_1 \sin\omega_2}{\cos\omega_2}$$

$$= \frac{(N_1 + U_1)\sin\omega_1 \cos\omega_2}{\cos\omega_2} + \frac{(N_1 + U_1)\cos\omega_1 \sin\omega_2}{\cos\omega_2}$$

$$= \frac{(N_1 + U_1)\sin(\omega_1 + \omega_2)}{\cos\omega_2} \quad (8)$$

thus

$$N_1 + U_1 = \frac{N\cos\omega_2}{\sin(\omega_1 + \omega_2)} \quad (9)$$

$$N_1 + U_1 + N_2 + U_2 = \frac{N\cos\omega_1}{\sin(\omega_1 + \omega_2)} + \frac{N\cos\omega_2}{\sin(\omega_1 + \omega_2)} = \frac{N(\cos\omega_1 + \cos\omega_2)}{\sin(\omega_1 + \omega_2)} \quad (10)$$

Assume $\lambda = \frac{\cos\omega_1 + \cos\omega_2}{\sin(\omega_1 + \omega_2)}$, $U = U_1 + U_2$, the equation will become to,

$$N_1 + N_2 = N\lambda - U \quad (11)$$

From equation (1), as

$$N = W\left(\cos\psi_p - k_h \sin\psi_p \pm k_v \cos\psi_p\right) + Q\cos\psi_p - k_h Q\sin\psi_p \pm k_v Q\cos\psi_p$$

Substitute *N* to equation (11), as

$$N_1 + N_2 = [W\left(\cos\psi_p - k_h \sin\psi_p \pm k_v \cos\psi_p\right) + Q\cos\psi_p - k_h Q\sin\psi_p \pm k_v Q\cos\psi_p]\lambda - U \quad (12)$$

References

Alejano, L. R., Ferrero, A. M., Ramirez-Oyanguren, P. and Alvarez Fernandez, M. I. (2011). Comparison of limit-equilibrium, numerical and physical models of wall slope stability. *International Journal of Rock Mechanics & Mining Sciences*, Vol. 48, No.1, pp. 16 – 26.

Adhikary, D. P., Muhlhaus, H – B. and Dyskin, A. V. (2001). A Numerical Study of Flexural Buckling of Foliated Rock Slopes. *International Journal for Numerical and Analytical Methods in Geomechanics*. Vol. 25, pp 871 - 884.

Aydan, O. and Kumsar, H. (2010). An experimental and theoretical approach on the modeling of sliding response of rock wedges under dynamic loading. *Rock Mechanics and Rock Engineering*, Vol. 43, No. 6, pp. 821 – 830.

Adhikary, D., Dyskin, A. V., Jewell, R. J. and Stewart, D. P. (1997). A study of the mechanism of flexural toppling failure of rock slopes. *Rock Mechanics and Rock Engineering*, Vol. 30, No. 2, pp. 75 – 93.

Hoek, E. and Bray, J. (1981). *Rock slope engineering*, 3rd Ed., Inst. Min. Metall., London.

Adhikary, D. P., Muhlhaus, H – B. and Dyskin, A. V. (2001). A Numerical Study of Flexural Buckling of Foliated Rock Slopes. *International Journal for Numerical and Analytical Methods in Geomechanics*. Vol. 25, pp 871 - 884.

Bobet, A. (1999). Analytical Solutions for Toppling Failure. *International Journal of Rock Mechanics & Mining Sciences*, Vol. 36, No.7, pp. 971 – 981.

Basha, B. M., ASCE, M. and Moghal, A. A. B. (2013). Load resistance factor design (LRFD) approach based seismic design of rock slope against wedge failure. Geo-Congress 2013, ASCE 2013.

Cavers, D. S. (1981). Simple methods to analyse buckling of rock slope. *Rock Mechanics*, Vol. 14, pp. 87-104.

Goodman, R. E. (1989) *Introduction to rock mechanics*, 2nd ed., Wiley, New York.

Goodman, R. E. and Shi, G. H. (1985). *Block theory and its applications to rock engineering*, Prentice-Hall, Englewood Cliffs, N.J.

Goodman, R. E. and Kieffer, S. D. (2000). Behavior of rock in slopes. *Journal of Geotechnical and Geoenvironmental Engineering*. Vol. 126, No. 8, pp 675 – 684.

He, L., An, X. M., Ma, G. W. and Zhao, Z. Y. (2013). Development of three – dimensional numerical manifold method for jointed rock slope stability analysis. *International Journal of Rock Mechanics & Mining Sciences*, Vol. 64, No.1, pp. 22 – 35.

Jimenez – Rodriguez, R., Sitar, N. and Chacon, J. (2006). System reliability approach to rock slope stability. *International Journal of Rock Mechanics & Mining Sciences*, Vol. 43, No.6, pp. 847 – 859.

Jimenez – Rodriguez, R. and Sitar, N. (2007). Technical note rock wedge stability analysis using system reliability mehthods. *Rock Mechanics and Rock Engineering*, Vol. 40, No. 4, pp. 419 – 427.

Kovari, K. and Fritz, P. (1975). Stability analysis of rock slopes for plane and wedge failure with aid of a programmable pocket calculator. 16th US Rock Mech. Symp., Minneapolis, USA, 25 – 33.

Kumsar, H., Aydan, O. and Ulusay, R. (2000). Dynamic and static stability assessment of rock slopes against wedge failures. *Rock Mechanics and Rock Engineering*, Vol. 33, No. 1, pp.

31 – 51.

Low, B. K., Member and ASCE. (1997). Reliability analysis of rock wedges. *Journal of Geotechnical and Geoenvironmental Engineering*, Vol. 123, No. 6, pp. 498 – 505.

Ling, H. I. and Cheng, A. H. -D. (1997). Rock sliding induced by seismic force. *International Journal of Rock Mechanics & Mining Sciences*, Vol. 34, No.6, pp. 1021 – 1029.

Low, B. K. (2007). Reliability analysis of rock slope involving correlated nonnormals. *International Journal of Rock Mechanics & Mining Sciences*, Vol. 44, No.6, pp. 922-935.

Ling, H. I. and Leshchinsky, D. (1995). Seismic performance of simple slopes. *Soils Foundations*, Vol. 35, No.2, pp. 85-94.

Nawari, O., Hartmann, R. and Lackner, R. (1997). stability Analysis of rock slopes with the direct sliding blocks method. *International Journal of Rock Mechanics & Mining Sciences*, Vol. 34:3-4, No.6, pp. 220.

Ohta, K. (1987). Geological structure of Unzen Volcano and its relation to the volcanic phenomena. Chidanken, Vol. 33, No.7, pp. 71-85.

Peter Bjerager. (1990). On computation methods for structural reliability analysis. *Journal of structure safety*, Vol. 9, No.9, pp. 79-96.

Shukla, S. K. and Hossain, M. M. (2011). Stability analysis of multi – directional anchored rock slope subjected to surcharge and seismic loads. *Soil Dynamics and Earthquake Engineering*. UK, DOI: 10.1016/j.soikdyn.2011.01.008

Tamimim, S., Amadei, B. and Frangopol, D. M. (1988). Mobte Carlo Simulation of Rock

Slope Reliability. *Computers & Structures*. Vol 33, No. 6, pp 1495 – 1505.

Terzaghi, K. (1963). Stability of steep slopes on hard, unweathered rock. *Geotechnique*, London, Vol. 12, No.4, pp. 251-270.

Wang, Y. – J., Yin, J. – H., Chen, Z. and Lee, C. F. (2004). Analysis of wedge stability using different methods. *Rock Mechanics and Rock Engineering*, Vol. 37, No. 2, pp. 127 – 150.

Wang, Y. – J. and Yin, J. – H. (2002). Technical note wedge stability analysis considering dilatancy of discontinuities. *Rock Mechanics and Rock Engineering*, Vol. 37, No. 2, pp. 127 – 137.

Wyllie, D.C. and Mah, C.W. (2004). *Rock slope engineering.* Fourth edition. London, Spon Press.

Yang, X. L., Li, L. and Yin, J. H. (2004). Stability analysis of rock slopes with a modified Hoek-Brown failure criterion. *International Journal of Numerical Analytical Methods Geomechanics* , Vol. 28, No.2, pp. 181-190.

Yang, X. L. and Zou, J. F. (2006). Stability factor for rock slopes subjected to pore water pressure based on the Hoek-Brown failure criterion. *International Journal of Rock Mechanics & Mining Sciences*, Vol. 43, No.7, pp. 1146-1152.